Bulletin of Mathematical Biology (2023) 85:64
https://doi.org/10.1007/s11538-023-01165-0

ORIGINAL ARTICLE

Rigorous Mapping of Data to Qualitative Properties of Parameter Values and Dynamics: A Case Study on a Two-Variable Lotka–Volterra System

Xiaoyu Duan[2] · Jonathan E. Rubin[1] · David Swigon[1]

Received: 19 December 2022 / Accepted: 2 May 2023

Abstract

In this work, we describe mostly analytical work related to a novel approach to parameter identification for a two-variable Lotka–Volterra (LV) system. Specifically, this approach is qualitative, in that we aim not to determine precise values of model parameters but rather to establish relationships among these parameter values and properties of the trajectories that they generate, based on a small number of available data points. In this vein, we prove a variety of results about the existence, uniqueness, and signs of model parameters for which the trajectory of the system passes exactly through a set of three given data points, representing the smallest possible data set needed for identification of model parameter values. We find that in most situations such a data set determines these values uniquely; we also thoroughly investigate the alternative cases, which result in nonuniqueness or even nonexistence of model parameter values that fit the data. In addition to results about identifiability, our analysis provides information about the long-term dynamics of solutions of the LV system directly from the data without the necessity of estimating specific parameter values.

Keywords Inverse problem · Parameter identification · Data fitting · Linear-in-parameters · Predator–prey

✉ David Swigon
swigon@pitt.edu

Xiaoyu Duan
xiaoyu.duan@nih.gov

Jonathan E. Rubin
jonrubin@pitt.edu

1 Department of Mathematics, University of Pittsburgh, 301 Thackeray Avenue, Pittsburgh, PA 15260, USA

2 Lab of Biological Modeling, National Institute of Diabetes and Digestive and Kidney Diseases, 12 South Dr., Bethesda, MD 20892, USA

Published online: 04 June 2023

1 Introduction

Lotka–Volterra models are ubiquitous in mathematical ecology, chemistry, and many other fields. Already by the 1970s, there was a vast literature on the dynamics of the Lotka–Volterra equations and their utility and limitations for modeling population data (May 1976; Wangersky 1978). This intensity of research effort reflects the centrality of the LV model and related constructs for ecological theory. Since then, related work has continued and expanded, including topics such as analysis of the behavior of LV systems, inclusion of stochasticity, delays, or spatial dependence, model generalizations, and various applications of the model.

Given a collection of measurements of the sizes or densities of co-existing populations at a discrete collection of time points, the LV system can, in theory, be used to predict the nature of the interactions between these populations, such as whether they are competitive or cooperative. To our knowledge, however, relatively little attention in the analysis of LV systems has been paid to the estimation of model parameters from data and to broader questions of parameter existence and identifiability for such systems (Wu and Wang 2011; Kloppers and Greeff 2013; Fort 2018; Khan and Chaudhary 2020; Lazzus et al. 2020).

These types of results are more challenging to obtain than one might initially think. When parameter estimation is performed in the process of modeling a biological system with an ordinary differential equation model, the starting point is the acquisition of a data set consisting of measurements taken at various times. The goal is to find a set of model parameter values and initial conditions for which the resulting model trajectory passes through the data points at the appropriate times. Typically that is accomplished using numerical optimization algorithms that minimize the discrepancy between model trajectories and observed data within a deterministic (Dalgaard and Larsen 1990; Kunze et al. 2004; Ramsay et al. 2007; Cao et al. 2011; Aster et al. 2018) or probabilistic setting (Tarantola, 2005; Calvetti and Somersalo, 2007; Evensen, 2009; Stuart, 2010; Smith, 2013; Calvetti and Somersalo, 2018). Approximation of derivatives from data and delayed embedding approaches has been also used (Packard et al. 1980; Takens 1981; Broomhead and King 1986). All such algorithms generally (i) require a large amount of data, (ii) provide parameter estimates whether the model is suitable for the biological system or not, and (iii) do not reveal possible alternative parameter fits. A naive counting argument suggests that for a model with p parameters and v variables such that v divides p, the parameters and initial conditions comprise a set of $p + v$ unknowns, and hence, we need $m + 1$ measurements of the model variables for $m = p/v$ to uniquely specify these unknowns. The problem of identifying parameters from data is nonlinear, however, even for model systems that are linear with respect to their state variables; hence, uniqueness and even existence of suitable parameter values can fail.

Because of the challenges associated with this nonlinear inverse problem, we have recently pursued a distinct alternative approach. Here, our aim is not to find the precise model parameter values (or ranges of such values) for which model trajectories come closest (or sufficiently close) to the data. Rather, we pursue *qualitative* information about the system that can be inferred from the available data. For example, such information can include conclusions about the existence or uniqueness of parameter values compatible with the data but can also relate to broader properties of parameters or trajectories. Such properties can include constraints on the signs or relative sizes of parameter values appearing in different terms in the model or information about whether model trajectories through the given data points must be periodic or bounded. Moreover, although such information is qualitative (e.g., the existence of parameter values rather than the values themselves), the analysis involved can be rigorous. Indeed, rigorous results detailing the properties of this formulation of the inverse problem have recently been obtained for linear systems by Stanhope et al. (2017) and affine systems by Duan et al. (2020). These studies provided information about the qualitative type of model interactions compatible with given data as well as analysis of how robust these results are to measurement error and small perturbations in model structure due, for example, to weak stochastic effects.

Most recently, numerical analysis of such questions for Lotka–Volterra systems has yielded some surprising results. For example, while it is well known that periodic cycling can emerge from predator–prey interactions, it has been demonstrated that methods associated with the qualitative inverse problem approach can determine whether a set of data points comes from a predator–prey system and whether this system is in an oscillatory regime, even when the data is too limited to capture multiple cycles (Duan et al. 2023). Here we present an analytical study of the inverse problem for that same Lotka–Volterra system in which we assume that three data points are given and ask whether one or more model parameter sets exist for which the trajectory passes through these data points, in a prescribed order, with the same fixed time of passage between each pair. Our analysis establishes a mapping between data and the system parameters for two instances of data: (i) three selected trajectory points equidistant in time or (ii) two trajectory points and the positive equilibrium. We show that in the second case, mapping from data to parameters is one-to-one, while in the first case, folds give rise to nonuniqueness. In both cases, there are data sets for which no parameter set exists that will reproduce them. Our approach yields a prediction about the nature of the species' interactions, such as whether they are engaged in a cooperative, competitive, or predator–prey type relationship, given the smallest necessary set of trajectory data. This is particularly useful for application to other biological systems for which the nature of interactions between components is variable in time.

The main purpose of this work is twofold. First, we seek to prove as many of the numerical findings obtained for the qualitative LV system inverse problem as possible. This step will place these findings on a firm mathematical footing, will clarify the system features from which they result, and hence will advance our understanding of the dynamics of the LV system and its utility for modeling. The ultimate goal in this direction, although not yet fully achieved, is to present a foundation for analysis of the LV system similar to that which we presented for linear (Stanhope et al. 2014, 2017) and affine (Duan et al. 2020) systems, whereby the model behaviors (such as periodicity or species persistence) are related directly to data via schematic diagrams without the need for precise parameter estimation. Second, the formulation of the LV system that we consider is both linear-in-parameters (LIP) and conservative, two properties that we define precisely in the next section and that we exploit heavily in our analysis. The presentation in this work should serve as a stepping stone to a more general theoretical understanding of issues related to parameter identifiability and inference of qualitative properties of parameters and solution trajectories for LIP systems, and possibly other nonlinear systems, especially the large class of other conservative model systems used across a broad range of fields (see, for example, MacKay and Meiss (2020)).

The remainder of this paper is organized as follows: In Sect. 2, we set up the inverse problem for a model LV system and review the numerical results obtained by Duan et al. (2023). In Sect. 3, we use the existence of conserved quantity to derive various results about geometrical properties of the trajectories of the system. In Sect. 4, we introduce and solve an alternative formulation of the qualitative inverse problem where the fixed point of the system replaces one of the data points. In Sect. 5, we show how various properties of the inverse problem solution, including nonexistence and nonuniqueness, can be deduced from results in Sects. 3 and 4. We close the paper with concluding remarks in Sect. 6.

2 Preliminaries on the Lotka–Volterra System and the Inverse Problem

Following Duan et al. (2023), we here focus on two-dimensional Lotka–Volterra system with no squared terms:

$$\begin{aligned} \dot{x} &= x(\alpha_1 + \beta_1 y), \\ \dot{y} &= y(\beta_2 x + \alpha_2), \\ x(0) &= x_0, \\ y(0) &= y_0, \end{aligned} \tag{1}$$

where the initial conditions x_0 and y_0 are assumed to be positive. The model generalizes the classical predator–prey model in that the rate constants $\alpha_1, \beta_1, \beta_2, \alpha_2$ are allowed to have arbitrary signs, to be later determined from given data. Regardless of the signs of the parameters, the first quadrant is invariant under the flow of (1); hence, we will focus on positive solutions.

The system (1) can be written in the formalism of linear-in-parameter (LIP) systems (Stanhope et al. 2014) as the vector ODE

$$\begin{aligned} \dot{\varphi} &= Af(\varphi), \\ \varphi(0) &= b, \end{aligned} \tag{2}$$

where the vector variable φ, coefficient matrix A, vector function $f(x, y)$ and vector of initial conditions b are defined as

$$\varphi = \begin{bmatrix} x \\ y \end{bmatrix}, \; A = \begin{bmatrix} \alpha_1 & \beta_1 & 0 \\ 0 & \beta_2 & \alpha_2 \end{bmatrix}, \; f(x, y) = \begin{bmatrix} x \\ xy \\ y \end{bmatrix}, \text{ and } b = \begin{bmatrix} x_0 \\ y_0 \end{bmatrix}. \tag{3}$$

Henceforth, we will also use the matrix A to represent the parameters $(\alpha_1, \beta_1, \beta_2, \alpha_2)$ of the system (1), making the implicit assumption that $a_{13} = a_{21} = 0$ in any such matrix A. We will use σ_A to denote the *signature of the system*, i.e.,

$$\sigma_A = [\mathrm{sgn}(\alpha_1) \quad \mathrm{sgn}(\beta_1) \quad \mathrm{sgn}(\beta_2) \quad \mathrm{sgn}(\alpha_2)], \tag{4}$$

such that σ_A specifies the types of interactions encoded by the model. In particular, positive values of both β_1 and β_2 indicate that the species engage in a cooperative interaction, negative values represent a competitive interaction, and distinct signs of β_1 and β_2 correspond to predator–prey interactions. As usual, for each species in isolation, α_1 and α_2 describe the intrinsic growth rate.

We are interested in parameter identification for system (2) from discrete data. In this context the term *forward problem* refers to finding a trajectory $\varphi = \varphi(t; A, b) : \mathbb{R} \times \mathbb{R}^{2\times 3} \times \mathbb{R}^2 \to \mathbb{R}^2$ to the IVP (2) for a given (A, b), from which we can in turn pick a set of times $\{t_0, t_1, \ldots, t_r\}$ and read off the data set $d = (P_0, P_1, \ldots, P_r) \in \mathcal{D}$, the data space, with $P_j = \varphi(t_j; A, b) \in \mathbb{R}^2$ for each j.

We here analyze the *inverse problem* for a given data set d, which refers to finding (A, b) such that the trajectory φ of (2) passes exactly through the points in a given data set, at the given times. This is not the same as the *data fitting problem*, which seeks an approximate trajectory of the system by optimizing the error between trajectory and data (Swigon et al. 2019). The inverse problem differs from data fitting problem in that while inclusion of too few data points in parameter inference leads to nonuniqueness of solutions, inclusion of too many data points leads to nonexistence of a solution.

As in Duan et al. (2023), we here address the solution of the inverse problem for system (1) for a specific choice of data for which the times are uniformly spaced (with $t_i = i$) and $d = (P_0, P_1, P_2)$, where the initial two points are fixed at $P_0 = (x_0, y_0)$ and $P_1 = (x_1, y_1)$ satisfying the following condition:

$$\text{(C)} \qquad x_1 > x_0 > 0 \text{ and } y_1 > y_0 > 0,$$

while the final data point $P_2 = (x_2, y_2)$ can lie anywhere in the first quadrant of the (x, y) plane. Note that condition (C) is not necessary for our analysis and can be replaced by other conditions such as $0 < x_1 < x_0$ and $y_1 > y_0 > 0$; that is, we assume that it holds for concreteness, but we can perform analogous analysis if given other such relationships. In Figure 10 of (Duan et al. 2023), we present numerical results for alternative choices of relative positions of P_0 and P_1 and provide a comparison between the specific results obtained numerically for these conditions.

We ask the following questions:

- *Existence* What is the set of values of P_2 for which there exists some A such that the system defined by (1) (or equivalently by (2)-(3)) has a trajectory $\varphi(t; A)$ with $P_j = \varphi(j, A)$, $j \in \{0, 1, 2\}$?
- *Uniqueness* What is the set of values of P_2 for which the parameter matrix A that solves the inverse problem is unique?
- *Parameter properties* When a solution of the inverse problem exists, what are the signs of the entries in A; that is, what is σ_A?

In the previous work, we investigated these questions numerically and obtained results that we can summarize in a single plot, which we call the P_2-*diagram* (Duan et al. 2023). In this diagram, shown here in Fig. 1, we consider the first quadrant of the (x, y)-plane as the set of possible locations of $P_2 = (x_2, y_2)$ under condition (C); hence, we label the axes as x_2, y_2. This plane is partitioned into disjoint, open regions, which we denote as $\mathcal{R}_\Omega$ for various Ω and which we label with these choices of Ω

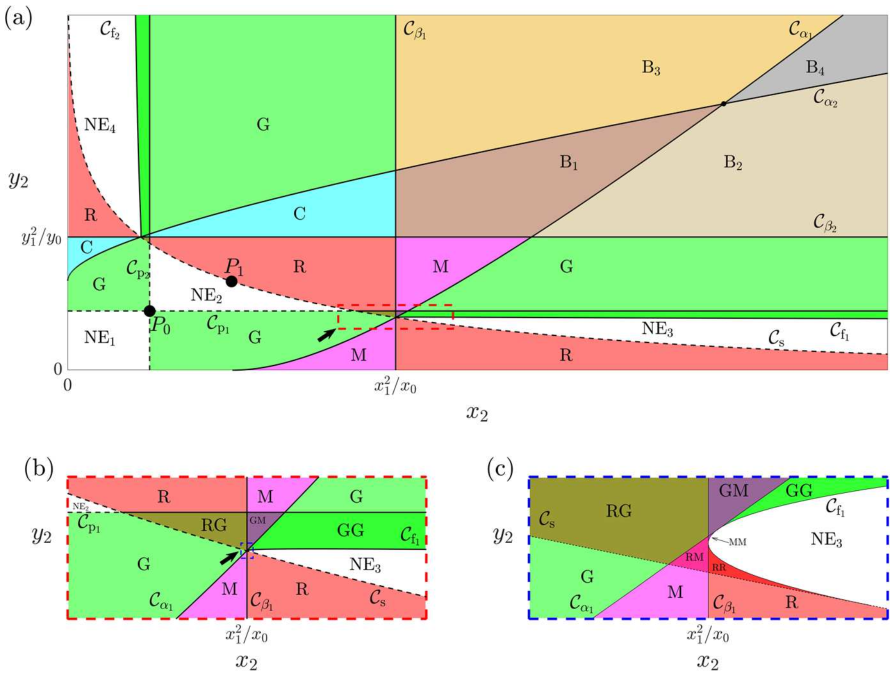

Fig. 1 The P_2-diagram, which depicts the regions $\mathcal{R}_\Omega$ of P_2 points for which the inverse problem has a specified signature σ_A (only the subscripts of the appropriate regions are shown), and shows the labels of the curves to be discussed in Sect. 5. Panels (**b**) and (**c**) are enlargements of the red and blue rectangles indicated by black arrows in panels (**a**) and (**b**), respectively. The data points P_0 and P_1 are fixed at the labeled positions. See text and Table 1 for more detailed descriptions of the regions (Color figure online)

in the diagram, in which the solution of the inverse problem appears to have distinct properties. Regions that share the same Ω and its corresponding color-coding represent choices of P_2 for which the inverse problem solution has the same properties. Specifically, Table 1 lists the σ_A values associated with all regions for which numerical analysis suggests that the inverse problem solution exists, along with the biological interpretations of these σ_A. The regions in the P_2-diagram on which the inverse problem solution does not exist are labeled by $\Omega = \mathrm{NE_i}$ for $i \in \{1, 2, 3, 4\}$, while other regions with double subscripts represent P_2 values where the solution exists but is not unique.

The major goal of this paper is to use mathematical analysis to establish rigorous proofs of various properties suggested from the numerical results shown in the P_2-diagram obtained by Duan et al. (2023) and thereby to provide better understanding and more complete characterization of the dynamics of system (1) and its dependence on observed data. We accomplish this aim by introducing a variant of the inverse problem in which the P_2 data point is replaced by P_*, the nontrivial equilibrium point. We show that in that case the inverse problem is uniquely determined by the data, and the dynamical behavior (i.e., the signature σ_A) is determined by simple explicit

Table 1 Properties of systems with $P_2 \in \mathcal{R}_\Omega$ of Fig. 1

Ω	# of solutions	σ_A	Dynamic type
R	≥ 1	$[+--+]$	Competitive
G	≥ 1	$[-+-+]$ or $[+-+-]$	Predator–prey
M	≥ 1	$[++-+]$	Parasitic
C	≥ 1	$[+-++]$	Parasitic
B_1	≥ 1	$[++++]$	Cooperative
B_2	≥ 1	$[-+++]$	Cooperative dependency
B_3	≥ 1	$[+++-]$	Cooperative dependency
B_4	≥ 1	$[-++-]$	Codependency
RR	≥ 2	$[+--+]$	Competitive
GG	≥ 2	$[-+-+]$ or $[+-+-]$	Predator–prey
MM	≥ 2	$[++-+]$	Parasitic
CC	≥ 2	$[+-++]$	Parasitic
RG	≥ 2	$[+--+]$ or $[-+-+]$ or $[+-+-]$	Competitive or predator–prey
GM	≥ 2	$[-+-+]$ or $[+-+-]$ or $[++-+]$	Predator–prey or parasitic
RM	≥ 2	$[+--+]$ or $[++-+]$	Competitive or parasitic
GC	≥ 2	$[-+-+]$ or $[+-+-]$ or $[+-++]$	Predator–prey or parasitic
RC	≥ 2	$[+--+]$ or $[+-++]$	Competitive or parasitic
NE	0		

criteria on P_*, as can be depicted in a P_*-diagram. We then relate the P_2-diagram to the P_*-diagram and show how nonuniqueness regions appear as folds.

Remark 1 As mentioned by Duan et al. (2023), in regions $\mathcal{R}_{\mathrm{G}}$ of the P_2-diagram, in which choices of P_2 correspond to periodic trajectories, time rescaling gives rise to countable families of matrices A that all solve the inverse problem. Thus, when we refer to the solution of the inverse problem in a case where the trajectory is periodic, we choose the matrix A for which the periodic trajectory reaches the point P_2 before returning to P_0, i.e., before completing a full orbit. We showed that this choice uniquely determines the signature of the inverse problem solution to be $\sigma_A = [-+-+]$ (and the trajectory travels clockwise) if P_2 is below the straight line P_0P_1, and $\sigma_A = [+-+-]$ (and the trajectory travels counterclockwise) if P_2 is above that line (Duan et al. 2023). In addition, with these assumptions, in the P_*-diagram described below, $\mathcal{R}_{\mathrm{G}_*}$ with $x_* > x_{01}$ corresponds to $\sigma_A = [-+-+]$, while $\mathcal{R}_{\mathrm{G}_*}$ with $x_* < x_{01}$ corresponds to $\sigma_A = [+-+-]$.

3 Hamiltonian and Specifics of the Inverse Problem

We start with some observations about useful properties of the LV system (1).

First, we note that when $\beta_1\beta_2 \neq 0$, system (1) has two equilibrium points, (0, 0) and

$$P_* = (x_*, y_*) = \left(-\frac{\alpha_2}{\beta_2}, -\frac{\alpha_1}{\beta_1}\right). \tag{5}$$

With (5), we can rewrite system (1) as

$$\begin{cases} \dot{x} = \beta_1 x(y - y_*), \\ \dot{y} = \beta_2 y(x - x_*), \\ x(0) = x_0, \\ y(0) = y_0. \end{cases} \tag{6}$$

Second, it is well-known and easy to check that system (1) is conservative, with the Hamiltonian function

$$H(x, y, A) = \alpha_2 \ln x + \beta_2 x - \alpha_1 \ln y - \beta_1 y = \beta_2(x - x_* \ln x) - \beta_1(y - y_* \ln y). \tag{7}$$

Since the level sets of the Hamiltonian represent orbits of system (1), one can use (7) to derive various relations between the constants in the model from known points on the trajectory. In particular for a trajectory passing through $P_0 = (x_0, y_0)$, any other point (x, y) on that trajectory obeys the following relation:

$$\beta_2\left(x - x_0 - x_* \ln\left(\frac{x}{x_0}\right)\right) = \beta_1\left(y - y_0 - y_* \ln\left(\frac{y}{y_0}\right)\right). \tag{8}$$

3.1 Known P_*

Consider a situation when in addition to P_0, P_1 the equilibrium point P_* of the system is given instead of the third data point P_2. For a trajectory passing through (P_0, P_1) (regardless of the timing or order of the passage), we have $H(x_0, y_0, A) = H(x_1, y_1, A)$, which, in view of (8), implies the following relation between the coordinates of P_0, P_1, the equilibrium P_*, and the ratio r of the constants β_2 and β_1 (provided $\beta_1 \neq 0$):

$$r = \frac{\beta_2}{\beta_1} = \frac{y_1 - y_0 - y_* \ln\left(\frac{y_1}{y_0}\right)}{x_1 - x_0 - x_* \ln\left(\frac{x_1}{x_0}\right)}. \tag{9}$$

Consequently, the inverse problem solution has nice properties, as indicated by the following result:

Theorem 1 *If the system* (1) *has a known equilibrium point* P_* *and a trajectory* $\varphi(t)$ *passing through points* P_0 *and* P_1 *(not necessarily at* $t = 0, 1$*), then its parameter matrix* A *is fixed to within a constant multiple and its orbit is specified uniquely. If, in* *addition, the timing of the passage of the trajectory between P_0 and P_1 is fixed, then A is specified uniquely and it depends continuously on P_*, P_0, P_1.*

Proof In view of (9) and the definitions of x_* and y_* given in (5), knowledge of P_0, P_1, P_* implies knowledge of the ratios of parameters $\frac{\beta_2}{\beta_1}, \frac{\alpha_2}{\beta_2}, \frac{\alpha_1}{\beta_1}$ and hence A is known to within a constant multiple. Furthermore, from (7), the orbit associated with the trajectory $\varphi(t)$ is determined uniquely by P_0, P_1, P_* and one can evaluate the line integrals along the orbit,

$$I_x = \int_{(x_0,y_0)}^{(x_1,y_1)} \frac{dx}{x(y-y_*)}, \qquad I_y = \int_{(x_0,y_0)}^{(x_1,y_1)} \frac{dx}{y(x-x_*)}. \tag{10}$$

Knowledge of $t_1 - t_0$ such that $P_i = \varphi(t_i), i = 0, 1$ can then be used to find $\beta_1 = I_x/(t_1 - t_0)$ or $\beta_2 = I_y/(t_1 - t_0)$, which determines A uniquely. The continuity of A follows from the continuous dependence of solutions of system (1) on parameters and on initial conditions. □

Theorem 1 can be used to derive a numerical method for estimating parameters of system (6) from a knowledge of two points P_0, P_1 on a trajectory and the equilibrium point P_* of the system. Although this problem is not a true “inverse problem" in the sense defined in Sect. 2, because it relies on information that is not contained in a trajectory of the system, it is still of practical utility. The solution (parameter matrix A) of such a problem is obtained by an algorithm that we denote as

$$A = \Psi_{P_* \to A}(P_*; P_0, P_1), \tag{11}$$

which we describe as follows:

Algorithm 1 ($\Psi_{P_* \to A}$)

Input: P_0, P_1, P_*.

1. Find r using (9).
2. Let $(\bar{\alpha}_1, \bar{\beta}_1, \bar{\beta}_2, \bar{\alpha}_2) = (-y_*, 1, r, -rx_*)$ and let $\bar{A}$ be the corresponding parameter matrix.
3. If the points P_0 and P_1 lie on the same branch of the Hamiltonian level set $H(x, y, \bar{A}) = H(x_0, y_0, \bar{A})$, then continue to the next step. If not, then there is no A for which (11) holds.
4. If the trajectory of (1) with matrix $\bar{A}$ starting at P_0 passes through P_1 as time increases, then continue to the next step. If not, then change $\bar{A}$ to $-\bar{A}$ and continue.
5. Let T be the smallest time at which the trajectory of (1) with $\bar{A}$ starting at P_0 passes through P_1. Let $A = T\bar{A}$ be the output of the algorithm.

Output: Parameter matrix A such that the system (1) has P_* as its equilibrium point and its trajectory $\varphi(t, A)$ obeys $P_j = \varphi(j, A)$ for $j = 0, 1$.

For each $P_* = (x_*, y_*)$, Algorithm 1 gives a parameter matrix $A = \Psi_{P_* \to A}(P_*; P_0, P_1)$. In theory, one can use it to try to solve the inverse problem by finding the point P_* for which (i) P_0, P_1, P_2 lie on the same branch of the level set $H(x, y, A) = H(x_0, y_0, A)$, (ii) the points P_0, P_1, P_2 lie in the proper order on the branch so that P_1 lies between P_0 and P_2, and (iii) the time of travel from P_0 to P_1

is the same as the time of travel from P_1 to P_2. It is important to note, however, that there are sets of (P_0, P_1, P_2) in the first quadrant for which no solution A exists and there are instances in which more than one solution exists.

3.2 Known P_2

Let us now return to the case when P_0, P_1, P_2 are given but P_* is not known. Note that (8) implies that $H(x_0, y_0, A) = H(x_1, y_1, A) = H(x_2, y_2, A)$ which yields the following result:

Theorem 2 *If the system (1) has a trajectory $\varphi(t)$ passing through points P_0, P_1, and P_2 (not necessarily at $t = 0, 1, 2$), then its parameter matrix A is an element of a 2D linear subspace defined by the constraint*

$$\begin{bmatrix} \ln(\frac{x_1}{x_0}) & x_1 - x_0 & y_0 - y_1 & \ln(\frac{y_0}{y_1}) \\ \ln(\frac{x_2}{x_1}) & x_2 - x_1 & y_1 - y_2 & \ln(\frac{y_1}{y_2}) \end{bmatrix} \begin{bmatrix} \alpha_2 \\ \beta_2 \\ \beta_1 \\ \alpha_1 \end{bmatrix} = 0$$

If, in addition, the timing of the passage of the trajectory between any two points among P_0, P_1, P_2 is fixed, then the trajectories passing through P_0, P_1, P_2 and their corresponding matrices A form a one-parameter family.

Proof The constraint follows immediately from (8) applied to the points P_0, P_1, P_2. Furthermore, the constraint can be turned into a relation that limits the extent of the location of the equilibrium point P_* of the system, i.e.,

$$\frac{y_2 - y_0 - y_* \ln\left(\frac{y_2}{y_0}\right)}{x_2 - x_0 - x_* \ln\left(\frac{x_2}{x_0}\right)} = \frac{y_1 - y_0 - y_* \ln\left(\frac{y_1}{y_0}\right)}{x_1 - x_0 - x_* \ln\left(\frac{x_1}{x_0}\right)}. \tag{12}$$

In particular, this relation shows that when trajectory passes through given P_0, P_1, P_2, one coordinate of P_* is a rational function of the other. In view of Theorem 1, for any choice of the coordinate x_* (or y_*), once the timing of the passage through the points P_0 and P_1 is fixed, both the trajectory $\varphi(t)$ and the corresponding matrix A are uniquely specified. □

Comparison of Theorem 1 with Theorem 2 reveals that supplementing knowledge of P_0 and P_1 with information about an additional point P_2 on the trajectory does not constrain the set of possible trajectories as much as providing information about the equilibrium point P_* of the system. To understand why the orbit of system (1) (or, equivalently, (6)) can be uniquely determined with a specification of P_0, P_1 and P_*, but not when only P_0, P_1 and P_2 are given, note that in the former case, the matrix A is an element of a 1D linear subspace defined by

$$\begin{bmatrix} \ln(\frac{x_1}{x_0}) & x_1 - x_0 & y_0 - y_1 & \ln(\frac{y_0}{y_1}) \\ 1 & x_* & 0 & 0 \\ 0 & 0 & y_* & 1 \end{bmatrix} \begin{bmatrix} \alpha_2 \\ \beta_2 \\ \beta_1 \\ \alpha_1 \end{bmatrix} = 0,$$

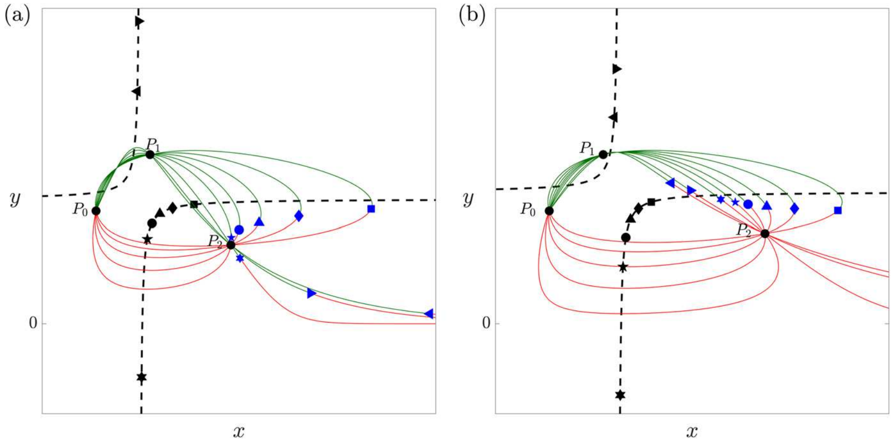

Fig. 2 Examples of orbits for families of trajectories passing through given data points P_0, P_1, P_2. Panels (**a**) and (**b**) correspond to two different choices of P_2. In each case, the families of equilibrium points given by (12) are shown as the dashed curves, the green segments of the trajectories correspond to $t \in [0, 2)$ while the red segments correspond to $t > 2$. The blue markers correspond to $t = 2$ on the trajectories; for each of these, there is a black marker of the same shape showing the position of the corresponding equilibrium point (Color figure online)

versus the 2D subspace defined in the statement of Theorem 2.

Relation (12) describes the one-parameter family from Theorem 2 as a family of equilibrium points P_*, parametrized by x_*, and the corresponding orbits that pass through P_0, P_1, P_2. Fixing the time of the passage from P_0 to P_1, however, does not imply that it will take the same time for the trajectory to pass from P_1 to P_2. In other words, the point $\varphi(2)$ will generally not be identical with the data point P_2 except for specific value(s) of x_*. It is possible that more than one x_* may lead to $P_2 = \varphi(2)$, which can result in nonuniqueness of the solution of the inverse problem.

In Fig. 2, we show examples of orbits for families of trajectories passing through points P_0, P_1, P_2. In both panels, we fix the same P_0 and P_1. The P_2 in panel (a) is chosen in the region $\mathcal{R}_{\mathrm{G}}$ with $x_1 < x_2 < x_1^2/x_0$ and $0 < y_2 < y_0$, and the P_2 in panel (b) is chosen in the region $\mathcal{R}_{\mathrm{NE}_3}$ (see Fig. 1). In each panel, we choose several P_* along the curve given by (12) (the dashed curve in the figure), and for each we use Algorithm 3.1 to obtain the corresponding parameter matrix A. With each A, we solve the system (1), sketch the trajectory, and mark the point $\varphi(2)$ on the trajectory (the blue markers in both panels). In panel (a) we note that the blue markers appear to make up a curve passing through P_2; when the blue marker is at P_2, the corresponding trajectory passes through P_2 at exactly $t = 2$, and hence we have a solution of the inverse problem. In panel (b), we note that the curve consisting of the blue markers does not pass through P_2, which seems to indicate that when P_2 is located in $\mathcal{R}_{\mathrm{NE}_3}$, there exists no trajectory that passes through P_i at $t = i$ for all three values $i = 0, 1, 2$.

4 Orbit Geometry and the P_*-diagram

4.1 Preliminaries

The primary goal of this paper is to establish the results depicted in the P_2-diagram in Fig. 1. We have seen in Sect. 3, however, that the location of the data (P_0, P_1, P_2), the location of the equilibrium point P_*, and the structure of the level sets of the Hamiltonian H are all strongly related.

In this section, we will take advantage of Theorem 1 and explore the existence, uniqueness, and properties of the solutions of a *modified* inverse problem where instead of the trajectory data (P_0, P_1, P_2) we are given (P_0, P_1, P_*). It turns out that by fixing P_0 and P_1 with $0 < x_0 < x_1$ and $0 < y_0 < y_1$ and studying how the properties of the level sets vary with P_*, we can extract a relation between the location of P_* and the sign structure σ_A of the system. We will present this idea here and then go on to classify the geometric structure of the level sets and to point out why some choices of P_* give no solution to the inverse problem. Subsequently, in Sect. 5 we translate the information gathered in this section to results in the setting of the P_2-diagram.

We begin by deriving some preliminary results. The level set (8) uses two functions in the form of

$$g(z) = g(z; a, b) := z - b - a \ln(z/b) \quad \text{with} \quad b > 0, \tag{13}$$

the properties of which are characterized by the following two lemmas that can be proved by analyzing the derivative of g.

Lemma 1 *Given any $a > 0$ and $b > 0$, the continuous function g strictly decreases from infinity on $(0, a)$, strictly increases to infinity on (a, ∞), and has a unique global minimum at $z = a$. The minimum value is negative when $a \neq b$ and zero when $a = b$. The graph of $g(z)$ has exactly two intersection points with any horizontal line above $g(a)$.*

Lemma 2 *Given any $a < 0$ and $b > 0$, the continuous function $g(z)$ strictly increases from negative infinity to positive infinity on $(0, \infty)$ and intersects the z-axis at $z = b$.*

Let $C_1(y_*) = r_{01}(y_* - y_{01})$ and $C_2(x_*) = x_{01} - x_*$ with

$$r_{01} = \frac{\ln(y_1/y_0)}{\ln(x_1/x_0)}, \qquad y_{01} = \frac{y_1 - y_0}{\ln(y_1/y_0)}, \qquad x_{01} = \frac{x_1 - x_0}{\ln(x_1/x_0)}. \tag{14}$$

The ratio r given by (9) can then be written as follows

$$r = -\frac{C_1(y_*)}{C_2(x_*)} = r_{01}\frac{y_* - y_{01}}{x_* - x_{01}}, \tag{15}$$

In view of (13) and (15), we can rewrite equation (8) for a level set passing through P_0 and P_1 as

$$F_i(x, y; x_*, y_*) = 0, \qquad i = 0, 1 \tag{16}$$

Table 2 Subregions of the P_*-diagram and associated sign signatures

Location of y_*	Location of x_* and σ_A		
	$(-\infty, 0)$	$(0, x_{01})$	(x_{01}, ∞)
(y_{01}, ∞)	$\mathcal{S}_1; [+-++]$	$\mathcal{S}_2; [+-+-]$	$\mathcal{S}_3; [+--+]$
$(0, y_{01})$	$\mathcal{S}_4; [-+++]$	$\mathcal{S}_5; [-++-]$	$\mathcal{S}_6; [-+-+]$
$(-\infty, 0)$	$\mathcal{S}_7; [++++]$	$\mathcal{S}_8; [+++-]$	$\mathcal{S}_9; [++-+]$

where

$$F_i(x, y; x_*, y_*) = C_1(y_*)g(x; x_*, x_i) + C_2(x_*)g(y; y_*, y_i), \qquad i = 0, 1. \quad (17)$$

We will often neglect to mention the dependence of F_i, C_1 and C_2 on (x_*, y_*) explicitly, but including this dependence explicitly will be useful in some of our analysis. Note that although the values of the function F_i at some (x, y) depend on the choice of i, the level set defined in (16) is independent of i. Since we will only need the level set and not the full function F_i, we shall drop the subscript on F.

4.2 General Observations

Let us now look at how the shape of the level set defined by (16), i.e., the shape of the curve on which there lies the orbit of a trajectory passing through points P_0 and P_1, depends on the location of the equilibrium point at P_*. In this section, we address the generic situation for which $\alpha_1, \beta_1, \alpha_2, \beta_2$ are all nonzero. Special cases with $\beta_1 = 0$ or $\beta_2 = 0$ (corresponding to points P_* at infinity) have explicit solutions and are discussed in Duan et al. (2023), while those with $\alpha_1 = 0$ or $\alpha_2 = 0$ (corresponding to points P_* on the axes) can be analyzed numerically using continuation methods. Based on the notation above and the definition of g in (13), equation (16) implies that if $x_* = x_{01}$, then the level set consists of two vertical lines $x = x_0$ and $x = x_1$, while if $y_* = y_{01}$, then the level set consists of two horizontal lines $y = y_0$ and $y = y_1$. In both cases, P_0 and P_1 lie on two distinct branches of the level set and hence there exists no solution to the inverse problem. Henceforth, we assume that $x_* \neq x_{01}$ and $y_* \neq y_{01}$.

The sign of r in (15) depends on the location of P_* relative to the vertical line $\{x = x_{01}\}$ and the horizontal line $\{y = y_{01}\}$. The signs of x_* and y_* affect the shape of the corresponding functions g in (17). Thus, the four lines, $x_* = 0$, $x_* = x_{01}$, $y_* = 0$, $y_* = y_{01}$, partition the $(x_*, y_*)-$plane into nine open rectangular regions, denoted for brevity as $\mathcal{S}_i$, $i \in \{1, \ldots, 9\}$, as defined in Table 2.

By the intermediate value theorem, we have $x_0 < x_{01} < x_1$ and $y_0 < y_{01} < y_1$. Therefore, P_0 and P_1 are always located in $\mathcal{S}_5$ and $\mathcal{S}_3$, respectively. Within each region $\mathcal{S}_i$ the signature σ_A of the system can take at most two values, as described by the following result:

Theorem 3 *Consider a system (6) with nonzero parameters $\alpha_1, \beta_1, \alpha_2, \beta_2$ and with a trajectory that passes through points P_0 and P_1 that obey condition (C). The equilib-*

rium point P_* and the signature σ_A are related by the following conditions (to within the ambiguity described in Remark 1):

- $\alpha_1 < 0 \Leftrightarrow y_* \in (0, y_{01})$
- $\beta_1 < 0 \Leftrightarrow y_* > y_{01}$
- $\beta_2 < 0 \Leftrightarrow x_* > x_{01}$
- $\alpha_2 < 0 \Leftrightarrow x_* \in (0, x_{01})$

Proof By Theorem 1, there is a unique orbit for any trajectory passing through P_0 and P_1 with given P_*. As we have mentioned above, there are no trajectories passing through both P_0 and P_1 when $x_* = x_{01}$ or $y_* = y_{01}$. By definition of P_*, when $x_* y_* = 0$, α_1 or α_2 is 0. Therefore, the regions $\mathcal{S}_1$, $\mathcal{S}_2$, ..., $\mathcal{S}_9$, shown in Table 2, cover all possible locations of P_* in the $x - y$ plane for a system (6) with nonzero parameters.

We first find σ_A for cases when P_* is not in the first quadrant by analysis of the vector field of system (6). Notice that the trajectory only lies in the first quadrant. When $y_* < 0$, $\dot{x}$ has the same sign as β_1 for all t, therefore $x_1 > x_0$ leads to $\beta_1 > 0$. A similar argument gives $\beta_2 > 0$ for $x_* < 0$. Using (15), we obtain the sign of $\beta_2 = \beta_1/r$ for $\mathcal{S}_8$ and $\mathcal{S}_9$, and likewise the sign of β_1 for $\mathcal{S}_1$ or $\mathcal{S}_4$. Finally, the signs of α_1 and α_2 in $\mathcal{S}_1, \mathcal{S}_4, \mathcal{S}_7, \mathcal{S}_8, \mathcal{S}_9$ can be determined by the definitions of x_* and y_* in (5).

When P_* is in the first quadrant, using similar analysis with (5) and (15), we can derive that

$$\sigma_A = \begin{cases} [+--+] \text{ or } [-++-], & \text{if } P_* \in \mathcal{S}_3 \cup \mathcal{S}_5 \\ [-+-+] \text{ or } [+-+-], & \text{if } P_* \in \mathcal{S}_2 \cup \mathcal{S}_6. \end{cases}$$

When $P_* \in \mathcal{S}_3$, we have $x_0 < x_*$ and $y_0 < y_*$ since $P_0 \in \mathcal{S}_5$. Thus, if $\sigma_A = [-++-]$, then $\dot{x}$ and $\dot{y}$ are negative at P_0 and in fact the trajectory is trapped in $(0, x_0) \times (0, y_0)$ for all positive t; hence, it cannot pass through P_1 at $t = 1$. Therefore, only $\sigma_A = [+--+]$ is possible. Similar analysis can be done to establish the unique sign signature for $P_* \in \mathcal{S}_2, \mathcal{S}_5$ or $\mathcal{S}_6$. □

Remark 2 Note that the conditions listed in Theorem 3 do not allow for $\alpha_1 < 0$ and $\beta_1 < 0$ simultaneously (or $\alpha_2 < 0$ and $\beta_2 < 0$ simultaneously). Thus, the signatures $\sigma_A = [----], [+---], [-+--], [++--], [--+-], [--++], [---+]$ are not compatible with our condition that the points P_0 and P_1 obey $x_0 < x_1$ and $y_0 < y_1$. These cases all lead to extinction of at least one species.

In the subsections below, we describe how the geometric structure of the level set of the Hamiltonian H that passes through points P_0 and P_1, as given by (16), depends on the location of P_*, and we illustrate the possible scenarios in Figs. 3 and 4. Finally, we will conclude this section with the P_*-*diagram*, shown in Fig. 5, which summarizes all of the information from this section. Specifically, the P_*-diagram displays the positions of the equilibrium point $P_* = (x_*, y_*)$ and the corresponding signature σ_A for trajectories $\varphi(t)$ that are potential solutions of the inverse problem, in the sense that $\varphi(i) = P_i$, $i = 0, 1$ and that $\varphi(2)$ exists and is located in the positive quadrant.

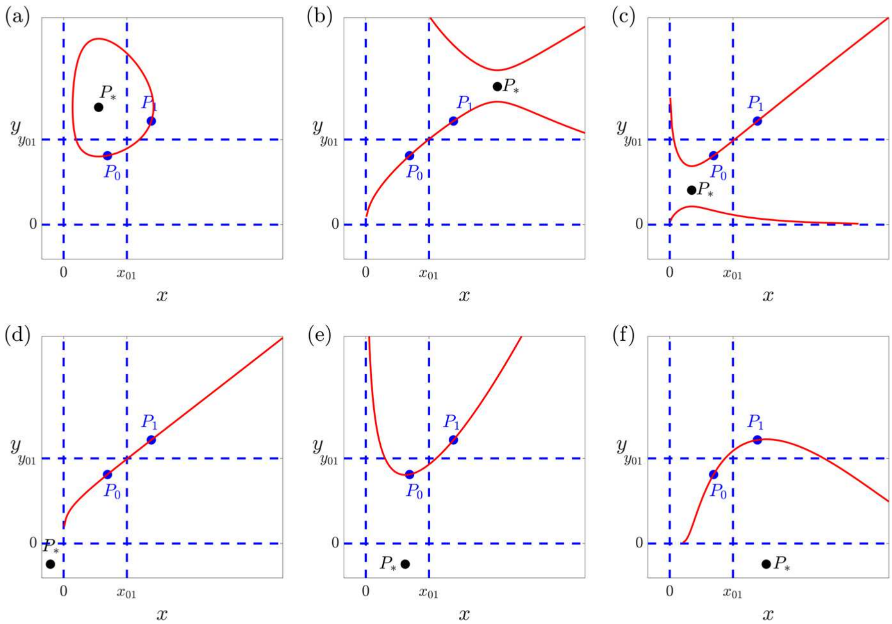

Fig. 3 Level sets $F(x, y; x_*, y_*) = 0$ corresponding to various locations of P_*. Symbols x_{01} and y_{01} are defined by (14). The four blue lines divide the plane into nine open regions $\mathcal{S}_i$ defined as in Table 2. (**a**) For P_* in $\mathcal{S}_2$, the zero level set of F is a closed curve. (**b**),(**c**) For P_* in $\mathcal{S}_3 \cup \mathcal{S}_5 \backslash \mathcal{T}$, with $\mathcal{T}$ defined by (18) whose properties are shown in subsection 4.4, the level set consists of two disjoint curves. Note that only the branch containing P_0 and P_1 is an orbit of a trajectory of system (1). (**d**),(**e**),(**f**) When $x_* < 0$ or $y_* < 0$, the level set consists of one connected curve

4.3 Case $P_* \in \mathcal{S}_2 \cup \mathcal{S}_6$

Theorem 4 *Let P_0 and P_1 obey condition (C). If $P_* \in \mathcal{S}_2 \cup \mathcal{S}_6$, then*

1. *the level set of the Hamiltonian is a closed curve bounded as $x_{r1} \le x \le x_{r2}$, $y_{r1} \le y \le y_{r2}$, where x_{r1}, x_{r2} are the solutions of $F(x, y_*; x_*, y_*) = 0$ and y_{r1}, y_{r2} are the solutions of $F(x_*, y; x_*, y_*) = 0$,*
2. *if $P_* \in \mathcal{S}_2$ and $y_* \le y_1$ ($y_* \ge y_1$), then the segment of the orbit with $y \ge y_1$ ($y \le y_1$) is a single-valued function of x on $[x_0, x_1]$,*
3. *if $P_* \in \mathcal{S}_6$ and $x_* \le x_1$ ($x_* \ge x_1$), then the segment of the orbit with $x \ge x_1$ ($x \le x_1$) is a single-valued function of y on $[y_0, y_1]$.*

Proof We focus on the case $P_* \in \mathcal{S}_2$ (see Fig. 3a) since for $P_* \in \mathcal{S}_6$ the argument is similar. In this case, x_*, y_*, C_1 and C_2 are all positive, so by Lemma 1, F attains a negative global minimum value at P_*, and strictly increases to infinity along every ray starting at P_* within the first quadrant. In other words, $z = F(x, y)$ is similar to an elliptic paraboloid with its minimum at P_*, but only defined in the first quadrant. Therefore, the zero level set of F is a closed curve within the first quadrant, convex (by Lemma 2.1 in Supplementary material of Duan et al. (2023)), passing through P_0 and P_1 and with P_* in its interior, and with extrema occurring at $x = x_*$ or $y = y_*$. At $x = x^*$, the y-coordinates of the orbit are the solutions y_{r2} and y_{r1} of

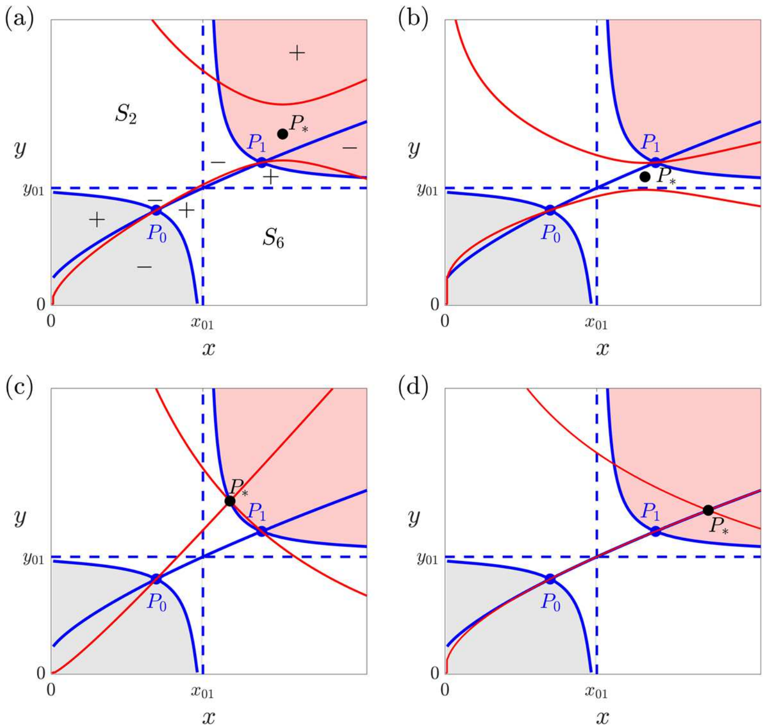

Fig. 4 Level sets $F(x, y; x_*, y_*) = 0$ (red curves) for various specific choices of P_*. Symbols x_{01} and y_{01} are defined by (14). The blue curves comprise the set $\mathcal{T}$. Here we use an example with $x_1 y_0 > x_0 y_1$ so $\mathcal{T}$ converges to the y-axis at two points and to the x-axis only at one point. Note that the regions in all four panels are identical, but we only show labels and signs of $Q(x, y)$ in (**a**) to avoid clutter. (**a**) With P_* in the red region, P_0, P_1 lie on the same branch of the level set, while P_* is not on the level set. (**b**) With P_* in a white + or a white − region, P_0, P_1 lie on different branches of the level set, while P_* is not on the level set. (**c**) In this case, $P_* \in \mathcal{T}_A$ and thus the level set consists of two curves intersecting at P_* with P_0, P_1 on different branches of the level set. (**d**) In this case, $P_* \in \mathcal{T}_C \subset \mathcal{T}$, and thus, the level set consists of two curves intersecting at P_* with P_0, P_1 on the same branch of the level set

$F(x_*, y; x_*, y_*) = 0$ and the orbit is bounded between those two values of y. The results about x_{r1} and x_{r2} can be derived similarly. Statements (2) and (3) follow from the convexity of the level set. □

An example of a level set with $P_* \in \mathcal{S}_2$ is shown in Fig. 3a. As we shall see below, the inverse problem has a solution for all $P_* \in \mathcal{S}_2 \cup \mathcal{S}_6$, and therefore, we shade the entire regions $\mathcal{S}_2, \mathcal{S}_6$ in the P_*-diagram in Fig. 5. In anticipation of further developments, we label these regions $\mathcal{R}_{\mathrm{G}_*}$ because when P_* lies in one of these regions, it will turn out that the corresponding P_2 for the trajectory lies in one of the components of $\mathcal{R}_{\mathrm{G}}$ in the P_2-diagram in Fig. 1.

4.4 Case $P_* \in \mathcal{S}_3 \cup \mathcal{S}_5$

When $P_* \in \mathcal{S}_3 \cup \mathcal{S}_5$, C_1 and C_2 have opposite signs, so $z = F(x, y)$ is similar to a hyperbolic paraboloid with saddle at P_* but only defined in the first quadrant. Thus,

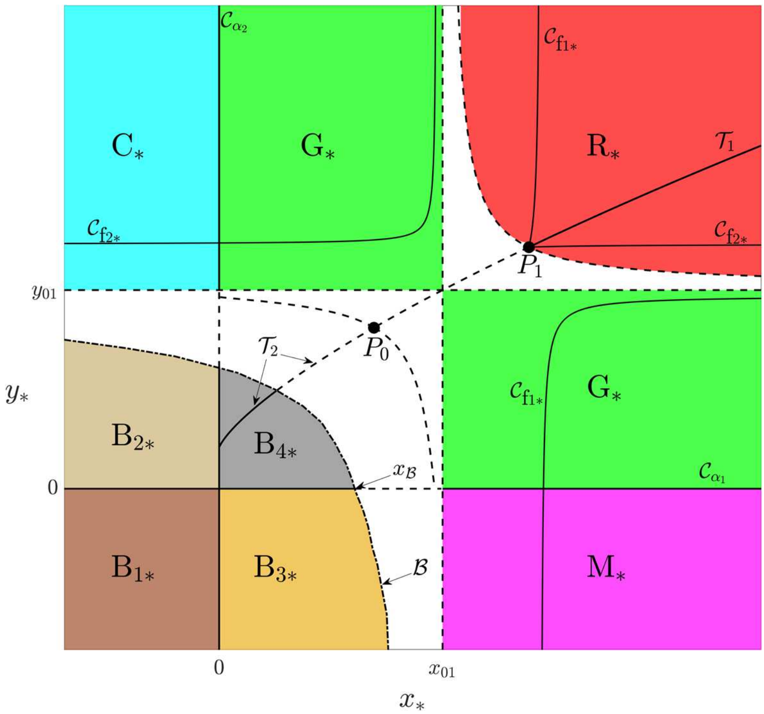

Fig. 5 The P_*-diagram depicting regions $\mathcal{R}_{\Omega_*}$ (only Ω_* labels are shown) for which system (6) has specified signature σ_A and has a trajectory $\varphi(t)$ that passes through P_0 and P_1 and stays finite at $t = 2$. The color-coding and labeling of regions match those of Fig. 1 and Table 1; for example, when P_* lies in $\mathcal{R}_{C_*}$, P_2 lies in $\mathcal{R}_C$. See text and Table 3 for more detailed descriptions of the regions. $\mathcal{B}$ is indicated with a dash-dotted curve, and $x_\mathcal{B}$ is its x-intercept

the level sets of such a function either consist of two disjoint curves or are made up of two curves that intersect transversally, which we address first. In order for the level set of $F(x, y; x_*, y_*) = 0$ to consist of two intersecting curves, both of those curves pass through the point of intersection (x_*, y_*). Let $\mathcal{T}$ be the set of all points P_* for which the level set of F is made up of two transversely intersecting curves,

$$\mathcal{T}:=\{(x_*, y_*) \mid F(x_*, y_*; x_*, y_*) = 0\}. \tag{18}$$

The set $\mathcal{T}$ is depicted in each panel of Fig. 4 as a collection of blue curves. Since it is central to our analysis, we characterize it in the following result, where, in view of (13) and (17), we define

$$Q(x, y) = F(x, y; x, y) = r_{01}(y - y_{01})h(x; x_1) + (x_{01} - x)h(y; y_1) \tag{19}$$

with

$$h(z; a):=g(z; z, a) = z - a - z\ln(z/a), \;\; z > 0, a > 0. \tag{20}$$

Lemma 3 *The set $\mathcal{T}$ has the following properties:*

1. *$\mathcal{T}$ consists of three curves, $\mathcal{T}_A$ and $\mathcal{T}_B$, each of which passes through one of the points P_0 or P_1, respectively, and $\mathcal{T}_C$ that passes through both of P_0 and P_1 as well as through the point (x_{01}, y_{01}). Each of the curves is defined by a single-valued function of either x or y.*
2. *Curve $\mathcal{T}_A$ has asymptotes $\lim_{x\to\infty} y = y_{01}$ from above and $\lim_{y\to\infty} x = x_{01}$ from the right. Curve $\mathcal{T}_B$ converges to the coordinate axes as follows: $\lim_{x\to 0} y = y_{\mathrm{r}} < y_{01}$, $\lim_{y\to 0} x = x_{\mathrm{r}} < x_{01}$. Curve $\mathcal{T}_C$ is monotone increasing with no asymptote and converges to a point on the x-axis if $x_1 y_0 - x_0 y_1 \le 0$, and to a point on the y-axis if $x_1 y_0 - x_0 y_1 \ge 0$.*
3. *$\mathcal{T}$ has two intersections with $\{x = b\}$ when $b \in (x_0, x_{\mathrm{r}}) \cup (x_{01}, x_1) \cup (x_1, \infty)$ and one intersection point when $b \in \{x_0\} \cup [x_{\mathrm{r}}, x_{01}] \cup \{x_1\}$; the number of intersection points with $\{x = b : b \in (0, x_0)\}$ depends on the sign of $x_1 y_0 - x_0 y_1$.*
4. *$\mathcal{T}$ is contained in $\mathcal{S}_3 \cup \mathcal{S}_5 \cup (x_{01}, y_{01})$ and separates each of the regions $\mathcal{S}_3$ and $\mathcal{S}_5$ into four open regions, with the signs of $Q(x_*, y_*)$ in each as shown in Fig. 4a.*

The proof is a straightforward application of properties of the functions $Q(x, y)$ and $h(z; a)$ defined in (19), (20), respectively. We can now demonstrate the geometric structure and some properties of the level sets $F(x, y; x_*, y_*) = 0$ for $P_* \in \mathcal{S}_3 \cup \mathcal{S}_5$.

Theorem 5 *Let P_0 and P_1 obey condition (C). If $P_* \in \mathcal{S}_3 \cup \mathcal{S}_5$, then the level set of the Hamiltonian has the following properties:*

1. *When $Q(x_*, y_*) > 0$, the level set of Hamiltonian is comprised of two disjoint curves, the upper curve $y = y_{\mathrm{U}}(x)$ bounded by $y_{\mathrm{r}2} \le y < \infty$ and the lower curve $y = y_{\mathrm{L}}(x)$ bounded by $0 < y \le y_{\mathrm{r}1}$, where $y_{\mathrm{r}1} < y_{\mathrm{r}2}$ are the solutions of $F(x_*, y; x_*, y_*) = 0$. The function $y_{\mathrm{U}}(x)$ decreases from infinity to $y_{\mathrm{r}2}$ on $(0, x_*]$ and increases to infinity on $[x_*, \infty)$, while $y_{\mathrm{L}}(x)$ increases from 0 to $y_{\mathrm{r}1}$ on $(0, x_*]$ and decreases to 0 on $[x_*, \infty)$.*
2. *When $Q(x_*, y_*) < 0$, the level set of the Hamiltonian is comprised of two disjoint curves that can be parametrized by y and classified as left and right branches. All other properties are analogous to case 1.*
3. *When $Q(x_*, y_*) = 0$, i.e., when $P_* \in \mathcal{T}$, the level set $F(x, y; x_*, y_*) = 0$ consists of two curves crossing at P_*.*

Proof Since $x_* > 0$, $y_* > 0$, Lemma 1 applies to both $g(x; x_*, x_0)$ and $g(y; y_*, y_0)$. We focus on the case $P_* \in \mathcal{S}_3$ since for $P_* \in \mathcal{S}_5$ the argument is similar. For $P_* \in \mathcal{S}_3$, $C_1 > 0 > C_2$ in (17) and, as a result, we have the following two observations: For fixed $\hat{x} > 0$ and $\hat{y} > 0$

$$F(\hat{x}, y; x_*, y_*) = 0 \text{ has } \left\{ \begin{array}{c} \text{two solutions } 0 < y_{\mathrm{r}1} < y_* < y_{\mathrm{r}2} \\ \text{a unique solution } y_* \\ \text{no solution } y \end{array} \right\}$$

$$\text{iff } g(\hat{x}; x_*, x_0) \left\{ \begin{array}{c} > \\ = \\ < \end{array} \right\} - \frac{C_2 h(y_*; y_0)}{C_1}; \tag{21}$$

$$F(x, \hat{y}; x_*, y_*) = 0 \text{ has } \begin{Bmatrix} \text{two solutions } 0 < x_{r1} < x_* < x_{r2} \\ \text{a unique solution } x_* \\ \text{no solution } x \end{Bmatrix}$$
$$\text{iff } g(\hat{y}; y_*, y_0) \begin{Bmatrix} > \\ = \\ < \end{Bmatrix} - \frac{C_1 h(x_*; x_0)}{C_2}. \tag{22}$$

If $Q(x_*, y_*) > 0$, then

$$h(y_*; y_0) < -C_1 h(x_*; x_0)/C_2. \tag{23}$$

In view of observation (21), for any $\hat{x} > 0$, $g(\hat{x}; x_*, x_0) \geq h(x_*; x_0) > -C_2 h(y_*; y_0)/C_1$, and hence, $F(\hat{x}, y; x_*, y_*) = 0$ has two distinct solutions, i.e., the level set has two distinct intersection points with every vertical line in the first quadrant. In particular, when $\hat{x} = x_*$,

$$g(y_{r_1}; y_*, y_0) = g(y_{r_2}; y_*, y_0) = -C_1 h(x_*; x_0)/C_2. \tag{24}$$

Lemma 1 gives $g(y; y_*, y_0) < -C_1 h(x_*; x_0)/C_2$ for $y \in (y_{r_1}, y_{r_2})$ and by observation (22), the level set of the Hamiltonian has no intersection with horizontal lines given by $y = \hat{y}$ with $\hat{y} \in (y_{r1}, y_{r2})$ and, in particular, with the line given by $y = y_*$. Finally, when $\hat{x} \to \infty$ or $\hat{x} \to 0^+$, $g(\hat{x}; x_*, x_0)$ approaches positive infinity, and hence, the solutions of $F(\hat{x}, y; x_*, y_*) = 0$ obey either $y \to \infty$ or $y \to 0^+$.

If $Q(x_*, y_*) < 0$, then a similar argument can be made with the roles of x and y reversed. In that case, the level set has two distinct intersection points with every horizontal line in the first quadrant and no intersections with vertical lines given by $x = \hat{x}$ with $\hat{x} \in (x_{r1}, x_{r2})$, where $g(x_{r_1}; x_*, x_0) = g(x_{r_2}; x_*, x_0) = -C_2 h(y_*; y_0)/C_1$. □

There is a further division of the regions $\mathcal{S}_3$ $\mathcal{S}_5$ by the set $\mathcal{T}$ depicted in Fig. 4. When P_* lies in the red or grey region, as in the panels (a) and (d) of Fig. 4, then P_0, P_1 belong to the same branch of the level set. If not, as in the panel Fig. 4b, then P_0, P_1 belong to different branches, in which case Algorithm 3.1 yields no output, and there is no solution to the inverse problem with such P_*. One can show these facts by using Theorem 5; for example, if P_* lies in the white + region as in the panel Fig. 4b, then by Theorem 5(a), the level set of the Hamiltonian is comprised of two disjoint curves with $y = y_*$ lying between them, so P_1 must belong to the upper curve (since $y_1 > y_*$) and similarly P_0 must belong to the lower curve. Therefore, for $P_* \in (\mathcal{S}_3 \cup \mathcal{S}_5)\backslash\mathcal{T}$, P_0 and P_1 lie on the same branch if and only if P_* is located in the region $\mathcal{U}$, which is the union of the four colored open regions in Fig. 4, defined as:

$$\mathcal{U} = \{(x_*, y_*) \in \mathcal{S}_3 \cup \mathcal{S}_5 \mid [(y_* - y_{01})Q(x_*, y_*) > 0 \wedge y_* \notin (y_0, y_1)] \\ \vee [(y_* - y_{01})Q(x_*, y_*) < 0 \wedge x_* \notin (x_0, x_1)]\}.$$

Note that $\mathcal{U}$ is disjoint from $\mathcal{T}$, the set where $Q(x_*, y_*) = 0$ (i.e., $\mathcal{U}$ does not include the blue curves in Fig. 4).

When $P_* \in \mathcal{T}$, the possibility of existence of a solution to the inverse problem arises only when P_* is located on either of the following components:

$$\mathcal{T}_1 = \mathcal{T} \cap ((x_1, \infty) \times (y_1, \infty)), \quad \mathcal{T}_2 = \mathcal{T} \cap ((0, x_1) \times (0, y_1)), \tag{25}$$

since only in these two cases P_0 and P_1 are on the same branch of an invariant manifold asymptotic to P_*. Otherwise, the points P_0 and P_1 lie on distinct arms of the level set, as in Fig. 4c.

In summary, when P_* is in the region $\mathcal{U}$, the level set of the Hamiltonian consists of two disjoint curves and both P_0 and P_1 lie on the same component (see Fig. 3b, c), while when $P_* \in (\mathcal{T}_1 \cup \mathcal{T}_2)$, the level set consists of two curves crossing at P_*, and both P_0 and P_1 lie on the same branch of an invariant manifold asymptotic to P_* (see Fig. 4d). We denote $\mathcal{R}_{\mathrm{R}_*} = \mathcal{S}_3 \cap (\mathcal{U} \cup \mathcal{T}_1)$.

4.5 Case $P_* \in \mathcal{S}_1, \mathcal{S}_4, \mathcal{S}_7, \mathcal{S}_8$, or $\mathcal{S}_9$

Theorem 6 *Let P_0 and P_1 obey the condition (C).*

1. *If $P_* \in \mathcal{S}_1$ then the level set of the Hamiltonian is a curve $x = x(y)$ defined for $y \in (0, \infty)$ with a single local maximum $x(y_*)$ and limits* $\lim_{y \to 0^+} x(y) = \lim_{y \to \infty} x(y) = 0$.
2. *If $P_* \in \mathcal{S}_4$ then the level set of the Hamiltonian is a curve $x = x(y)$ defined for $y \in (0, \infty)$ with a single local minimum $x(y_*)$ and limits* $\lim_{y \to 0^+} x(y) = \lim_{y \to \infty} x(y) = \infty$.
3. *If $P_* \in \mathcal{S}_7$ then the level set of the Hamiltonian is a monotone increasing curve in x and y.*
4. *If $P_* \in \mathcal{S}_8$ then the level set of the Hamiltonian is a curve $y = y(x)$ defined for $x \in (0, \infty)$ with a single local minimum $y(x_*)$ and limits* $\lim_{x \to 0^+} x(y) = \lim_{x \to \infty} x(y) = \infty$.
5. *if $P_* \in \mathcal{S}_9$ then the level set of the Hamiltonian is a curve $y = y(x)$ defined for $x \in (0, \infty)$ with a single local maximum $y(x_*)$ and limits* $\lim_{x \to 0^+} x(y) = \lim_{x \to \infty} x(y) = 0$.

Proof The proof is similar to that of Theorem 5. When x_* or y_* is negative, Lemma 2 characterizes the corresponding g function in F. For example, if $P_* \in \mathcal{S}_k$, $k = 7, 8, 9$, then $y_* < 0$. By Lemma 2, for any $\hat{x} \in (0, \infty)$, $F(\hat{x}, y; x_*, y_*) = 0$ has a unique solution, so the level set is a simple, connected, continuous curve. □

In each of the regions $\mathcal{S}_1$ and $\mathcal{S}_9$, every point P_* produces a level set that passes though both points P_0 and P_1. In Fig. 5, we label $\mathcal{S}_1$ and $\mathcal{S}_9$, respectively, as $\mathcal{R}_{\mathrm{C}_*}$ and $\mathcal{R}_{\mathrm{M}_*}$ (although only C_*, M_* labels are shown).

4.6 Consequences of the Order of Points on a Trajectory

When a third data point P_2 on a trajectory is available, a question arises as to whether the order of the points on the level set corresponds to the order of times at which the trajectory passes through those points. Many different possibilities could be explored here; however, we only focus on the following result that will be used later.

Proposition 1 *Let P_0 and P_1 obey the condition (C). Suppose that there exists a trajectory $\varphi(t) = (x(t), y(t))$ passing through P_0, P_1, and P_2 at times $t_0 < t_1 < t_2$, respectively.*

1. *If $P_2 \in (0, x_1] \times (0, y_1]$, then $P_* \in \mathcal{S}_2 \cup \mathcal{S}_6$ and the orbit is closed.*
2. *If $P_2 \in (x_1, \infty) \times (0, y_1)$, then P_* must lie in one of the following: $\mathcal{S}_2$, $\mathcal{S}_6$, $(x_{01}, \infty) \times \{0\}$, $\mathcal{S}_9$, or in the red + region in Fig. 4 panel (a).*

Proof For part (1), if P_* is located in $\mathcal{S}_i$ with $i \neq 2$ and $i \neq 6$, then by Theorem 5 and Theorem 6, either $x(t)$ or $y(t)$ is monotone along the trajectory $\varphi(t)$. If $x_* = 0$, then $\dot{y} = \beta_2 xy$ remains the same sign in the first quadrant, which makes $y(t)$ monotone. Similarly, $y_* = 0$ leads to monotonicity of $x(t)$. Therefore, either $x_1 < x(2)$ or $y_1 < y(2)$ and P_2 cannot be located in $(0, x_1] \times (0, y_1]$. The fact that the orbit is closed follows from Theorem 4.

For part (2), suppose that $P_2 \in (x_1, \infty) \times (0, y_1)$, then P_* cannot be located in $(-\infty, x_{01}) \times (-\infty, y_{01})$, since after $\varphi(t)$ passes through P_1, both $x(t)$ and $y(t)$ are monotone increasing. Similarly, we can exclude the case when $x_* \leq 0$, since $y(t)$ is always monotone increasing by $\dot{y} = \beta_2 y(x - x_*)$ and condition (C). Finally, if $P_* \in \mathcal{S}_3$, then P_* must be in the red region in Fig. 4 so that the trajectory passes through both P_0 and P_1, and P_* cannot be in the red − region since in that case $y(t)$ is monotone increasing. The remaining possibilities are exactly those given in the result statement. ◻

4.7 Consequences of Timing of Trajectories

Up to this point, we have analyzed the geometry of the level sets of the Hamiltonian and eliminated regions in the P_* plane for which the corresponding level set does not include a curve that passes through both P_0 and P_1. However, if we additionally require that the P_* location corresponds to the existence of a solution to the inverse problem, then the trajectory $\varphi(t)$ of the system (6) with $P_i = \varphi(i)$, $i = 0, 1$ must exist for times up to $t = 2$.

When $P_* \in \mathcal{S}_2 \cup \mathcal{S}_6$, the level set is a closed curve and the trajectory can be extended for $t \to \infty$. When $P_* \in \mathcal{T}_1$, then both points P_0 and P_1 lie on a stable manifold of the equilibrium P_*, and hence, the point $\varphi(2)$ lies on $\mathcal{T}_1$ between P_1 and P_*. Note that no solution exists for $P_* \in \mathcal{T} \setminus (\mathcal{T}_1 \cup \mathcal{T}_2)$ including $P_* = P_0$.

When $P_* \in \mathcal{T}_2$, the situation is more complicated, since the solution might go to infinity before time $t = 2$; therefore, the region of possible P_* locations with $\sigma_A = [- + +-]$ is a subset of $\mathcal{S}_5 \cap (\mathcal{U} \cup \mathcal{T}_2)$. The basic argument is as follows: The points P_0, P_1 are on the unstable manifold of P_*. We can transform the system to straighten the unstable manifold and in the neighborhood of P_* the rate of motion away from P_*, based on the unstable eigenvalue, is $\lambda := \sqrt{\beta_1 \beta_2 x_* y_*}$. Thus, if we take an initial condition that is $O(\epsilon)$ from the critical point, the time to travel an $O(1)$ distance scales as $(1/\lambda) \ln(1/\epsilon)$. To make this time itself equal to 1 requires $\lambda \sim \ln(1/\epsilon)$. But

Table 3 Definitions of the regions $\mathcal{R}_{\Omega_*}$ in the P_*-diagram and signs of parameters in each

$\mathcal{R}_{\Omega_*}$	σ_A
$\mathcal{R}_{\mathrm{R}_*} = (\mathcal{U} \cap \mathcal{S}_3) \cup \mathcal{T}_1$	$[+--+]$
$\mathcal{R}_{\mathrm{G}_*} = \mathcal{S}_2 \cup \mathcal{S}_6$	$\pm[-+-+]$
$\mathcal{R}_{\mathrm{M}_*} = \mathcal{S}_9$	$[++-+]$
$\mathcal{R}_{\mathrm{C}_*} = \mathcal{S}_1$	$[+-++]$
$\mathcal{R}_{\mathrm{B}_{1*}} = \{(x_*, y_*) \in \mathcal{S}_7 \mid$ the trajectory does not blow up before time 2$\}$	$[++++]$
$\mathcal{R}_{\mathrm{B}_{2*}} = \{(x_*, y_*) \in \mathcal{S}_4 \mid$ the trajectory does not blow up before time 2$\}$	$[-+++]$
$\mathcal{R}_{\mathrm{B}_{3*}} = \{(x_*, y_*) \in \mathcal{S}_8 \mid$ the trajectory does not blow up before time 2$\}$	$[+++-]$
$\mathcal{R}_{\mathrm{B}_{4*}} = \{(x_*, y_*) \in (\mathcal{U} \cap \mathcal{S}_5) \cup \mathcal{T}_2 \mid$ the trajectory does not blow up before time 2$\}$	$[-++-]$

a nonlinear system of the form $\dot{x} = c\ln(1/\epsilon)x(y - y_*)$, $\dot{y} = \ln(1/\epsilon)y(x - x_*)$ blows up at time $t = 1/(\ln(1/\epsilon)) < 1$. By moving P_* away from P_0 along $\mathcal{T}_2$, we notice that the blow-up time increases until it equals $t = 2$. We can think of the trajectory at this point as a solution to a boundary value problem (BVP) for a compactified version of (6) with a boundary condition at the image of infinity at time $t = 2$. By continuing this BVP with respect to the parameter x_*, we obtain a curve $y_*(x_*)$ that defines systems for which a solution exists such that $\varphi(i) = P_i$, $i = 0, 1$ and blow-up occurs at $t = 2$. This curve lies inside $\cup_{i\in\{4,5,7,8\}}\mathcal{S}_i$. On one side of this curve, a solution to the inverse problem exists while on the other side it does not. We denote this curve as

$$\mathcal{B} = \{(x_*, y_*) \mid \inf\{\bar{t} : \lim_{t\to\bar{t}} \varphi(t; P_*) = \infty\} = 2\}.$$

4.8 Summary

At this point, we can summarize the information that we have established about the relation between the location of P_* and the existence and sign signatures of solutions of system (6) in the P_*-diagram displayed in Fig. 5. To complement the P_*-diagram, the definitions of the labeled regions $\mathcal{R}_{\Omega_*}$ and their corresponding σ_A are shown in Table 3, where we have used the fact that $\mathcal{T}_2 \subset \mathcal{S}_5$ and hence $\mathcal{S}_5 \cap (\mathcal{U} \cup \mathcal{T}_2) = (\mathcal{U} \cap \mathcal{S}_5) \cup \mathcal{T}_2$.

If P_* is located in any white region or on a dashed curve, then there exists no A such that the system has a trajectory $\varphi(t)$ that passes from P_0 to P_1 in one time unit and remains finite at $t = 2$. Notice that the solid segments within the curve $\mathcal{T}$ that passes through P_0 and P_1 are $\mathcal{T}_1$ and a portion of $\mathcal{T}_2$ as defined in (25) and correspond to locations of P_* for which P_0 and P_1 lie on the same branch of the level curve and the timing condition can be satisfied, such that a solution to the inverse problem exists (cf. Figure 4). Moreover, within the regions $\mathcal{S}_7$, $\mathcal{S}_4$, $\mathcal{S}_8$, and $\mathcal{S}_5$, we have defined subregions $\mathcal{R}_{\mathrm{B}_{1*}}$, $\mathcal{R}_{\mathrm{B}_{2*}}$, $\mathcal{R}_{\mathrm{B}_{3*}}$, and $\mathcal{R}_{\mathrm{B}_{4*}}$, respectively, on which the solution does not blow up before time 2, as shown in Table 3.

5 The P_2-diagram and the Solution of the Inverse Problem

Now we return our focus to the inverse problem introduced in Sect. 2 and the description of the P_2-diagram in Fig. 1. Recall that Algorithm 3.1 gives a unique parameter matrix A for any P_* that lies in the appropriate region of the P_*-diagram once the timing of the passage from P_0 to P_1 is specified. Since A is determined uniquely, the trajectory $\varphi(t)$ of the system (1) obeying $P_i = \varphi(i)$ for $i = 0, 1$ with equilibrium at P_* is likewise unique, and the point $P_2 = \varphi(2)$ is therefore determined uniquely as well by (P_0, P_1, P_*). In addition, note that the trivial nonuniqueness of A based on time rescaling for periodic solutions, discussed previously, does not affect the location of $\varphi(2)$. We formalize these observations in terms of the continuous map

$$P_2 = \Psi_{P_* \to P_2}(P_*; P_0, P_1) \tag{26}$$

that takes a subset of $\mathbb{R}^2$ into $\mathbb{R}^2_+$ (a consequence of the dynamics being restricted to the first quadrant). For any choice of fixed P_0, P_1, we can also visualize the map $\Psi_{P_* \to P_2}$ as a 2-dimensional manifold $\mathcal{M}$ in the 4-dimensional space $\mathbb{R}^2 \times \mathbb{R}^2_+$. The projection of this manifold onto $\mathbb{R}^2$ provides the P_*-diagram, while the projection onto $\mathbb{R}^2_+$ gives the P_2-diagram.

The study of the P_*-diagram in Sect. 4 provides a starting point for analysis of the manifold $\mathcal{M}$. As we shall see below, the map $\Psi_{P_* \to P_2}$ is not one-to-one and hence the manifold $\mathcal{M}$ has folds that show up in the P_2-diagram. Each region $\mathcal{R}_{\Omega_*}$ in the P_*-diagram is mapped continuously onto the corresponding region $\mathcal{R}_{\Omega}$ in the P_2-diagram. Regions $\mathcal{R}_{\Omega_1}$, $\mathcal{R}_{\Omega_2}$ for some choices of Ω_1, Ω_2 may overlap, however, giving rise to regions that we denote by $\mathcal{R}_{\Omega_1\Omega_2}$ in the P_2-diagram.

Some conjectures about the solution of the inverse problem for the system (1) under condition (C) have been presented in detail in Duan et al. (2023), are shown schematically in Fig. 1, and can be summarized as follows:

1. The first quadrant can be partitioned into open regions $\mathcal{R}_{\Omega}$ in which there are solutions to the inverse problem with a particular sign structure σ_A of A. Regions labeled by the same subscript and shown in the same color share the same sign structure for A, as indicated in Table 1.
2. If $P_2 \in \mathcal{R}_{\mathrm{NE}} = \cup_{j=1}^4 \mathcal{R}_{\mathrm{NE}_j}$, then the inverse problem has no solution.
3. If P_2 is located in any labeled region $\mathcal{R}_{\Omega}$ not included in $\mathcal{R}_{\mathrm{NE}}$ except for regions $\mathcal{R}_{\mathrm{G}}$ or regions labeled with two letters, or P_2 lies on any boundary between regions represented by a solid curve in the P_2-diagram, then the inverse problem has a unique solution.
4. In regions $\mathcal{R}_{\mathrm{G}}$ the inverse problem has a countable family of solutions that correspond to periodic orbits.
5. In regions $\mathcal{R}_{\Omega}$ labeled by two letters (but not by NE), two solutions arise due to a fold in the manifold $\mathcal{M}$.
6. The existence of region $\mathcal{R}_{\mathrm{B}_4}$ depends on the magnitude of x_0, y_0, x_1, y_1.
7. The regions are separated by the curves of vanishing parameters $\mathcal{C}_{\alpha_1}$, $\mathcal{C}_{\alpha_2}$, $\mathcal{C}_{\beta_1}$, $\mathcal{C}_{\beta_2}$, the separatrix $\mathcal{C}_{\mathrm{s}}$, the periodic orbit limits $\mathcal{C}_{\mathrm{p}_1}$, $\mathcal{C}_{\mathrm{p}_2}$ and the fold curves $\mathcal{C}_{\mathrm{f}_1}$, $\mathcal{C}_{\mathrm{f}_2}$.
8. The curves $\mathcal{C}_{\mathrm{s}}$, $\mathcal{C}_{\mathrm{p}_1}$, and $\mathcal{C}_{\mathrm{p}_2}$ correspond to limiting cases where one or several parameters blow up.

These results have been obtained numerically by continuation methods and it makes sense to ask whether there are rigorous justifications for them. We now turn to presenting such justifications for a subset of these conjectures.

We begin our theoretical analysis with some preliminary results that we found useful for considering the nonexistence of a solution to the inverse problem and then we derive results on (non)existence, uniqueness, and parameter-dependence of solutions. As noted in the proof of Theorem 3.1, given P_0, P_1 and P_* with $\beta_1\beta_2 \neq 0$, integration of system (1) rewritten in the form (6) yields two potential equations for passage times along a trajectory from a point (x_a, y_a) to a point (x_b, y_b), as follows:

$$t_{a\to b} = \int_{x_a}^{x_b} \frac{dx}{\beta_1 x(y-y_*)} = \int_{y_a}^{y_b} \frac{dy}{\beta_2 y(x-x_*)}. \tag{27}$$

When an orbit can be locally parametrized by x or y, one can evaluate or estimate the time $t_{a\to b}$ in (27), using the first or the second equation, respectively. The terms $x - x_*$ and $y - y_*$ in the path integrals suggest that we should investigate the distance between the points on the level set of the Hamiltonian and the critical point P_* along either of the coordinate directions. Using this idea, we obtain the following results.

Lemma 4 *Consider a level set (8) of the Hamiltonian determined by P_0, P_1, and P_*. Whenever this set intersects a line $y = \bar{y}$ at two distinct points $(x_{r1}, \bar{y})$ and $(x_{r2}, \bar{y})$ with $x_{r2} > x_{r1}$, it follows that $x_{r2} > x_* > x_{r1}$ and $x_{r2} - x_* > x_* - x_{r1}$. A similar result holds for intersections of the level set with a line $x = \bar{x}$.*

Proof We only show the case with a horizontal line since the vertical case is similar. If the level set intersects with the line $y = \bar{y} > 0$ at $(x_{r1}, \bar{y})$ and $(x_{r2}, \bar{y})$ with $x_{r2} > x_{r1}$, then x_{ri}, $i = 1, 2$ are roots of the equation

$$f(x){:=}r\left(x - x_1 - x_* \ln\left(\frac{x}{x_1}\right)\right) = \bar{y} - y_1 - y_* \ln\left(\frac{\bar{y}}{y_1}\right).$$

Since $f(x)$ is a convex function and x_* is a minimum of $f(x)$, we have $x_{r2} > x_* > x_{r1} > 0$. Furthermore, $f(x_{r2}) - f(x_{r1}) = x_{r2} - x_{r1} - x_* \ln\left(\frac{x_{r2}}{x_{r1}}\right) = 0$. To complete the proof, it suffices to show that $x_{r2} + x_{r1} > 2x_*$, which follows from the inequality $\frac{b+a}{2} > \frac{b-a}{\ln b - \ln a}$. To show that this inequality holds for any two distinct positive numbers a and b, fix $a > 0$ and let $h(x) = \frac{x+a}{2}(\ln x - \ln a) - (x - a)$ for $x > a$. Compute $h''(x) = \frac{1}{2x}(1 - \frac{a}{x})$, so h' decreases when $x < a$ and increases on $x > a$, with a global minimum at $x = a$. Moreover, $h'(x) = \frac{1}{2}(\ln x - \ln a) + \frac{a}{2x} - \frac{1}{2}$, so $h'(a) = 0$ and $h'(x)$ is always positive for $x > a$. Therefore h is monotone increasing, and hence when $x > a$, $h(x) > h(a) = 0$, and choosing $x = b$ gives $\frac{b+a}{2} > \frac{b-a}{\ln b - \ln a}$. □

Lemma 4 implies the following.

Corollary 1 *Given x_* and one point, say (x_0, y_0), on the orbit of the system (1), there exists another point $(\bar{x}_0, y_0)$ on that orbit as well, where $\bar{x}_0$ satisfies $x_0 - \bar{x}_0 - x_* \ln(x_0/\bar{x}_0) = 0$, which is independent of y_*. Therefore, if we vary P_* vertically* *and generate different orbits of the system that pass through* (x_0, y_0)*, then they all pass through* $(\bar{x}_0, y_0)$ *as well. A similar argument can be made for another point* $(x_0, \bar{y}_0)$ *when we move* P_* *horizontally.*

With Lemma 4, we can also derive the following theorem, which is applied in proving a result about nonexistence of solutions to the inverse problem later in this section.

Theorem 7 *Let* Γ *be a trajectory of system (1) inside the first quadrant. Consider a vertical strip* $\{x_a < x < x_b : x_a > 0\}$ *that is intersected by* Γ *in two distinct arcs. Then*

1. *one of the arcs lies above* $y = y_*$ *and one below,*
2. Γ *travels in opposite* x*-directions along the upper and lower arcs, and*
3. *if* T_U *and* T_L *are the passage times for* Γ *along the upper and lower arcs, respectively, then* $T_U < T_L$.

Proof Part (1) follows from our observation that any trajectory Γ is a level set of the Hamiltonian, and the fact that the points at which $y = y_*$ are the extrema of the level set when viewed as a function of y. Part (2) follows directly from the flow equation $\dot{x} = \beta_1 x(y - y_*)$. To prove part (3), we will assume without loss of generality that $\beta_1 > 0$, so the flow goes from right to left along the lower arc of Γ. By construction, each of the two arcs can be parametrized in x, and we consider the upper and lower arcs as the graphs of functions that we denote by $y_U(x)$ and $y_L(x)$, respectively. We have

$$T_U = \int_{x_a}^{x_b} \frac{dx}{\beta_1 x(y_U(x) - y_*)} \quad \text{and} \quad T_L = \int_{x_b}^{x_a} \frac{dx}{\beta_1 x(y_L(x) - y_*)}.$$

By Lemma 4, for any $x \in (x_a, x_b)$, $y_U(x) - y_* \geq y_* - y_L(x) > 0$, so $\beta_1 T_U < \beta_1 T_L$. Therefore $T_U < T_L$ because $\beta_1 > 0$. The proof is similar when $\beta_1 < 0$. □

Similarly, we have the following corollary for intersections with a horizontal strip.

Corollary 2 *Let* Γ *be a trajectory of (1) inside the first quadrant. Consider a horizontal strip* $\{y_a < y < y_b : y_a > 0\}$ *such that its intersection with* Γ *consists of two disconnected arcs. Then one of those arcs lies to the left of* $x = x_*$ *and the other to the right, the* y*-direction of* Γ *is opposite in the left and right arcs, and for the passage times* T_r *and* T_l *of* Γ *along the right and left arcs, respectively, we have* $T_r < T_l$.

5.1 Separatrix $\mathcal{C}_s$

The Hamiltonian and associated results make it possible to find analytical results about the separatrix $\mathcal{C}_s$, which we identified numerically in Duan et al. (2023) and which, we shall see, relates to the transition between nonexistence and existence of inverse problem solutions.

Consider the limiting case of a system (1) with $P_* = P_1$, in which case the level set of the Hamiltonian becomes $F(x, y; x_1, y_1) = 0$, where F is defined in equations

(13)-(17). This level set, uniquely defined by the locations of P_0 and P_1, consists of two curves that intersect at P_1 transversely, one of which passes through P_0 and extends to infinity in the direction of increasing x and y. The other curve is the separatrix $\mathcal{C}_s$. For the system with $P_* = P_1$, both curves are invariant manifolds of the flow, asymptotic to P_1, and P_0 lies on the stable one. It follows that the trajectory of a system (1) with equilibrium point $P_* = P_1$ starting at P_0 cannot reach P_1 in finite time but instead converges to P_1 as time goes to infinity. As a result, the system can have no trajectory passing through P_0, P_1 when $P_2 \in \mathcal{C}_s$. Thus, in the P_2-diagram, parts of the separatrix $\mathcal{C}_s$ lie on boundaries between the regions of existence and nonexistence of the solution of the inverse problem. The graph of $\mathcal{C}_s$ is shown in panel (a) of Fig. 1 as the dashed line going from the top left corner to the bottom right corner, forming the boundary between the red regions $\mathcal{R}_R$ and the white regions $\mathcal{R}_{NE_4}$, $\mathcal{R}_{NE_2}$, and $\mathcal{R}_{NE_3}$.

To see what happens to the parameters $\alpha_1, \beta_1, \beta_2, \alpha_2$ in the limit as $P_* \to P_1$, note that for $P_* = P_1$, the manifold from P_0 to P_1 can be parametrized by x between x_0 and x_1 and by y between y_0 and y_1. Therefore, in (10), as $P_* \to P_1$, $I_x \to -\infty$ and $I_y \to -\infty$, which implies that $\beta_1, \beta_2 \to -\infty$ with their ratio r approaching $r_{01} \frac{y_1 - y_{01}}{x_1 - x_{01}}$, while, in view of (5), $\alpha_1, \alpha_2 \to \infty$. We conclude that the entire curve $\mathcal{C}_s$ is the image of the single point P_1 under the map $\Psi_{P_* \to P_2}$ and that several of the values of $\alpha_1, \beta_1, \beta_2, \alpha_2$ approach infinity as $P_2 \to \mathcal{C}_s$.

The separatrix $\mathcal{C}_s$ has an intersection with the vertical line $x = x_1^2/x_0$. In the following lemma, we prove that condition (C) implies that this intersection point is always below the horizontal line $y = y_0$. Similarly, $\mathcal{C}_s$ intersects the line $y = y_1^2/y_0$ to the left of $x = x_0$.

Lemma 5 *Assume that condition (C) holds. Then, the intersection of $\mathcal{C}_s$ and $\{x = x_1^2/x_0\}$ occurs at a value $y_{S\beta_1}$ that is smaller than y_0.*

Proof The value $y_{S\beta_1}$ is the smaller solution of the equation

$$y - y_1 - y_1 \ln\left(\frac{y}{y_1}\right) = r_{01} \frac{y_1 - y_{01}}{x_1 - x_{01}} \left(\frac{x_1^2}{x_0} - x_1 - x_1 \ln\left(\frac{x_1}{x_0}\right)\right). \tag{28}$$

By the properties of the function $g(y; y_1, y_1)$ stated in Lemma 4.1, it suffices to show that $g(y_{S\beta_1}; y_1, y_1) > g(y_0; y_1, y_1)$, which is equivalent to

$$\left(\frac{x_1^2}{x_0} - x_1 - x_1 \ln\left(\frac{x_1}{x_0}\right)\right) > \left(x_0 - x_1 - x_1 \ln\left(\frac{x_0}{x_1}\right)\right) \tag{29}$$

since $r_{01} \frac{y_1 - y_{01}}{x_1 - x_{01}} > 0$. Notice that the function $u - \frac{1}{u} - 2\ln u$ is monotone increasing on $(0, +\infty)$ and is 0 only at $u = 1$. Therefore when $u = \frac{x_1}{x_0} > 1$, we have $u - \frac{1}{u} - 2\ln u > 0$, which is equivalent to (29). ◻

5.2 Conditions for Nonexistence of Solutions

In this section we establish necessary and sufficient conditions on data that one can use to quickly identify whether the data are compatible with the system in the sense that the inverse problem has a solution. Specifically, we apply the preliminary results established at the start of this section to establish the nonexistence of solutions to the inverse problem when P_2 lies in $\mathcal{R}_{\mathrm{NE}_1}$ or $\mathcal{R}_{\mathrm{NE}_2}$.

Theorem 8 *(Nonexistence-1) If $P_2 \in \mathcal{R}_{\mathrm{NE}_1} = ((0, x_0] \times (0, y_0]) \setminus P_0$, then no solution of the inverse problem exists.*

Proof Consider the Hamiltonian level set defined by P_0, P_1 and let $P_2 \in ((0, x_0] \times (0, y_0]) \setminus P_0$. By Proposition 1(1), the level set is a closed orbit with $\sigma_A = \pm[- + -+]$ and with $0 < x_* < x_0$ or $0 < y_* < y_0$. Without loss of generality, suppose that $\sigma_A = [- + -+]$ (so the trajectory is traversed clockwise) and hence $0 < y_* < y_0$. The closed orbit intersects the vertical strip $x_0 < x < x_1$ in two arcs, where the upper one represents a complete orbit between P_0 and P_1 while the lower one represents a subsegment of the orbit between P_1 and P_2. In view of Theorem 7, the time of travel along the upper arc T_U is smaller than the time of travel along the lower arc T_L. This property is incompatible with the existence of a trajectory $\phi(t)$ that passes through P_0, P_1, P_2 at times $t = 0, 1, 2$, respectively, since such a trajectory would require $T_U = 1 > T_L$. □

The region $\mathcal{R}_{\mathrm{NE}_2}$ is bounded by the separatrix $\mathcal{C}_s$ and the lines $\{y = y_0\}$ and $\{x = x_0\}$. It includes its three boundary curve segments but does not include the point P_0. We will now prove the nonexistence of solutions to the inverse problem when P_2 lies in $\mathcal{R}_{\mathrm{NE}_2}$. Using the lines $\{y = y_1\}$ and $\{x = x_1\}$, we separate $\mathcal{R}_{\mathrm{NE}_2}$ into three regions, the rectangular region $\mathcal{R}^{(1)}_{\mathrm{NE}_2} := ([x_0, x_1] \times [y_0, y_1]) \setminus P_0$ and two triangle-like regions, denoted as $\mathcal{R}^{(2)}_{\mathrm{NE}_2}$ (bounded above by $\mathcal{C}_s$, at the bottom by $\{y = y_0\}$, and on the left by $\{x = x_1\}$) and $\mathcal{R}^{(3)}_{\mathrm{NE}_2}$ (bounded above by $\mathcal{C}_s$, at the bottom by $\{y = y_1\}$, and on the left by $\{x = x_0\}$). We only prove nonexistence for $P_2 \in \mathcal{R}^{(1)}_{\mathrm{NE}_2}$ and $P_2 \in \mathcal{R}^{(2)}_{\mathrm{NE}_2}$, since the symmetry of x and y in system (1) and in the inverse problem imply that the proof for $\mathcal{R}^{(3)}_{\mathrm{NE}_2}$ is similar to the latter.

Theorem 9 *(Nonexistence-2) If $P_2 \in \mathcal{R}^{(1)}_{\mathrm{NE}_2}$, then no solution of the inverse problem exists.*

Proof By Proposition 1(1), if there exists a trajectory for such P_2 with parameter matrix A, then the orbit is closed. We decompose the rectangular region $\mathcal{R}^{(1)}_{\mathrm{NE}_2}$ into two triangles based at the diagonal $P_0 P_1$ and assume that P_2 is in the upper triangle (including the top and left boundaries, but not the diagonal since that is ruled out by the convexity of the orbit, as established in previous work (Duan et al. 2023)). As stated in Remark 1, we choose the A with the greatest possible transit time along the orbit and for this orbit, the flow proceeds counterclockwise with $\sigma_A = [+ - +-]$. Moreover, the flow is monotone decreasing in x from P_1 to P_2. Now we consider the vertical strip $[x_2, x_1] \times (0, \infty)$ whose intersection with the orbit consists of an upper arc connecting P_1 and P_2 and a lower arc that is contained in the trajectory from P_0 to P_1 and hence has a passage time of less than 1. By Theorem 7, the passage time for the flow along the upper arc is less than that along the lower arc and hence is less than 1, which leads to a contradiction. A similar contradiction occurs if P_2 is in the lower triangle relative to $P_0 P_1$. □

Theorem 10 *(Nonexistence-3) If $P_2 \in \mathcal{R}^{(2)}_{\mathrm{NE}_2}$, then no solution of the inverse problem exists.*

Proof To establish a contradiction, suppose that $P_2 \in \mathcal{R}^{(2)}_{\mathrm{NE}_2}$ and there exists a solution A. By Proposition 1(2), the corresponding equilibrium point P_* must lie in $\mathcal{R}_{\mathrm{G}_*}$, on $(x_{01}, \infty) \times \{0\}$, in $\mathcal{R}_{\mathrm{M}_*}$, or in the subset of $\mathcal{R}_{\mathrm{R}_*}$ given by the red + region in Fig. 4a. These are displayed as the colored regions in Fig. 6a. Since $\mathcal{R}^{(2)}_{\mathrm{NE}_2}$ is below the straight line $P_0 P_1$, following Remark 1, if $P_* \in \mathcal{R}_{\mathrm{G}_*}$, then we choose A that yields clockwise passage from P_0 to P_1 to P_2. Therefore all possible positions of P_* have $x_* > x_{01}$ and then by Theorem 3, $\beta_2 < 0$. (Hence in Fig. 6b–d we only color the regions to the right of x_{01}.)

We first establish that $x_* > x_1$. Suppose the contrary, then the trajectory starting at P_0 increases in y until $x = x_*$, then decreases in the y direction, passes through P_2, and intersects with $\{y = y_0\}$ again. Consider the horizontal strip $(0, \infty) \times [y_0, y_1]$ as shown in Fig. 6b, in which P_2 therefore lies. The trajectory intersects this strip in two arcs, and we denote the passage time for the flow along the left and right arcs as T_l and T_r, respectively. By Corollary 2, $T_r < T_l \leq 1$, which contradicts the fact that the passage time from P_1 to P_2, which must be less than or equal to T_r, is equal to 1. Thus, we have $x_* > x_1$.

Now we prove that when $x_* > x_1$ and $P_* \in \cup_{\Omega \in \{\mathrm{R,G,M}\}} \mathcal{R}_{\Omega_*}$, the trajectory does not have any intersection with $\mathcal{R}^{(2)}_{\mathrm{NE}_2}$. It suffices to show that within the horizontal strip $[x_1, \infty) \times [y_0, y_1]$, the trajectory lies to the right of $\mathcal{C}_{\mathrm{s}}$ (as sketched in Fig. 6c, where the horizontal dashed line is $\{y = \hat{y}\}$, and the diagonal dashed curve is $\mathcal{C}_{\mathrm{s}}$). Given $x_* > x_1$, for any $\hat{y} \in [y_0, y_1]$, the trajectory intersects the line $\{y = \hat{y}\}$ in two points with $x \geq x_0$. We are interested in the intersection point on the right and denote it as $(\hat{x}, \hat{y})$, so $\hat{x} > x_* > x_1$. We will show that both the partial derivatives $\frac{\partial \hat{x}}{\partial x_*}$ and $\frac{\partial \hat{x}}{\partial y_*}$ are positive when P_* is located in any of those possible regions we mentioned at the beginning of the proof.

From the equation (8) with r given by (15), we have that

$$\frac{\hat{x} - x_*}{\hat{x}} \frac{\partial \hat{x}}{\partial x_*} = \ln\left(\frac{\hat{x}}{x_1}\right) - \frac{1}{r_{01}} \frac{g(\hat{y}; y_*, y_1)}{y_{01} - y_*}$$

and

$$\frac{\hat{x} - x_*}{\hat{x}} \frac{\partial \hat{x}}{\partial y_*} = \frac{x_{01} - x_*}{r_{01}} \frac{g(\hat{y}; y_{01}, y_1)}{(y_* - y_{01})^2}$$

where g is given by equation (13) and r_{01} as defined previously is positive. We first focus on $\partial \hat{x}/\partial y_*$. By Lemma 1, $g(\hat{y}; y_{01}, y_1)$ is negative when $\hat{y} \in (y_0, y_1)$ and zero

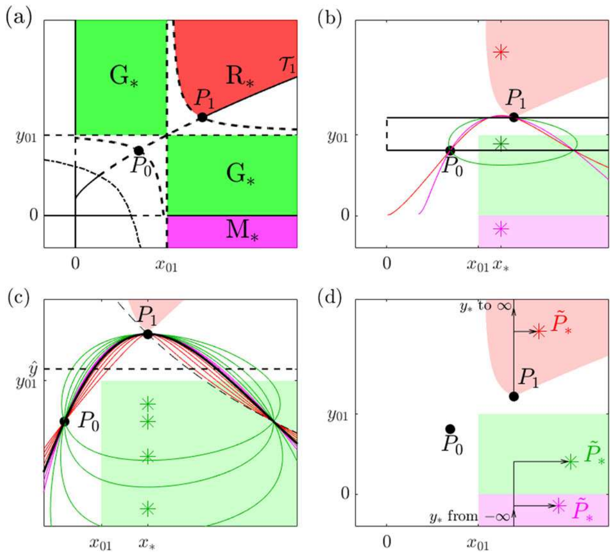

Fig. 6 Four plots for the proof of Theorem 10. They are identical (except that in (c) we zoom in to see the details of trajectories), but we only show necessary symbols in each panel to avoid clutter. Note that asterisks denote locations of the equilibrium point P_* for the trajectories shown in (b), (c); see text for additional details

when $\hat{y} = y_0$ or $\hat{y} = y_1$. Therefore in the setting of this proof, $\partial\hat{x}/\partial y_*$ is positive when $\hat{y} \in (y_0, y_1)$ and is zero when $\hat{y} = y_0$ or $\hat{y} = y_1$. (The case when $\hat{y} = y_0$ is consistent with Remark 1.)

Next we study $\partial\hat{x}/\partial x_*$. The term $\ln\left(\hat{x}/x_1\right)$ is always positive so it suffices to show that $g(\hat{y}; y_*, y_1)/(y_{01} - y_*)$ is never positive. This is obvious if $y_* = 0$, so we discuss the other three cases of possible values of y_* corresponding to the competitive, predator–prey, and parasitic cases (with red, green and magenta colors in Fig. 5, respectively):

1. If $y_* > y_{01}$, then $y_* > y_1$. By Lemma 1, $g(\hat{y}; y_*, y_1)$ is positive when $\hat{y} \in (0, y_1)$.
2. If $0 < y_* < y_{01} < y_1$, then $\ln(\hat{y}/y_1) < 0$ and hence $g(\hat{y}; y_*, y_1) < g(\hat{y}; y_{01}, y_1) \leq 0$.
3. If $y_* < 0$, then by Lemma 2, $g(\hat{y}; y_*, y_1) < 0$.

Thus, in all cases, $\partial\hat{x}/\partial x_*$ is indeed positive.

Before we can use these derivative results, we add one more observation: if we fix $x_* = x_1$ and any $\hat{y} \in [y_0, y_1]$ and vary $y_* \in (-\infty, y_{01}) \cup (y_1, \infty)$, the orbit will change accordingly and will have different intersection points with the horizontal line $y = \hat{y}$, so the corresponding $\hat{x}$ will change. But in both of the limits $y_* \to \infty$ and $y_* \to -\infty$, the defining equation for the orbit tends to

$$\frac{r_{01}}{x_* - x_{01}}\left(x - x_1 - x_* \ln\left(\frac{x}{x_1}\right)\right) = -\ln\left(\frac{y}{y_1}\right),$$

which is the solid black curve in Fig. 6c. Hence, with $y = \hat{y}$ fixed, the same $\hat{x}$ value, given by the solution of this equation, results.

Putting together this observation and the derivative results, we can finish the proof. Recall that $\mathcal{C}_\text{s}$ can be treated as the limiting case of the trajectory when $P_* = P_1$, so if the equilibrium point is actually at some $\tilde{P}_*{:=}(\tilde{x}_*, \tilde{y}_*)$ in the red + region as in Fig. 4a (and with $\tilde{x}_* > x_1$), then the corresponding trajectory can be obtained from $\mathcal{C}_\text{s}$ by first fixing $x_* = x_1$ and increasing y_* from y_1 to $\tilde{y}_*$, and then fixing $y_* = \tilde{y}_*$ and increasing x_* from x_1 to $\tilde{x}_*$. By the analysis of the signs of $\partial\hat{x}/\partial x_*$ and $\partial\hat{x}/\partial y_*$, for each $\hat{y} \in [y_0, y_1]$, the corresponding $\hat{x}$ is nondecreasing through the vertical shifting process and strictly increasing through the horizontal one. Thus, the trajectory corresponding to equilibrium point $\tilde{P}_*$ is on the right of $\mathcal{C}_\text{s}$ while it crosses through the horizontal strip $[x_1, \infty) \times [y_0, y_1]$. If $\tilde{P}_*$ is in $\mathcal{R}_{\text{G}_*}$ or $\mathcal{R}_{\text{M}_*}$, then we replace the process by first fixing $x_* = x_1$ and increasing y_* from y_1 to ∞ (throughout which process $\hat{x}$ does not decrease), and then fixing $x_* = x_1$ and increasing y_* from $-\infty$ to $\tilde{y}_*$, using our observation that the $\hat{x}$ for $y_* \to -\infty$ is also the $\hat{x}$ for $y_* \to \infty$, and finally fixing $y_* = \tilde{y}_*$ and increasing x_* from x_1 to $\tilde{x}_*$ (throughout which process $\hat{x}$ strictly increases). This process is shown in Fig. 6d. So we again conclude that the trajectory corresponding to the equilibrium point $\tilde{P}_*$ is on the right of $\mathcal{C}_\text{s}$ in the horizontal strip $[x_1, \infty) \times [y_0, y_1]$, as desired. □

At this time, we do not have analytical results about the nonexistence of solutions for P_2 in the regions $\mathcal{R}_{\text{NE}_3}$ and $\mathcal{R}_{\text{NE}_4}$, primarily because we do not have a good handle on the boundaries of those regions. Although one of the boundaries is the separatrix, $\mathcal{C}_\text{s}$, the other boundaries are the fold curves $\mathcal{C}_{\text{f}_1}, \mathcal{C}_{\text{f}_2}$, which were computed using a numerical approach (see Duan et al. (2023) for detail) and remain to be analytically characterized in future work.

5.3 Determination of Dynamical Behavior from Data

In this section, we prove a necessary and sufficient condition on data that one can use to identify the signature of the system and hence the types of interactions governing the observed species. Specifically, the sign of β_2 for $P_2 \in [x_1, \infty) \times [y_1, \infty)$ is given by the following theorem:

Theorem 11 *If a solution to the inverse problem exists for a value* $P_2 \in [x_1, \infty) \times [y_1, \infty)$*, then the sign of* β_1 *is equal to that of* $x_2 - x_1^2/x_0$ *and the sign of* β_2 *is equal to that of* $y_2 - y_1^2/y_0$*.*

Proof We only show that $x_2 \geq x_1^2/x_0$ if and only if $\beta_1 \geq 0$, since the proof of the other statement is similar.

In Subsection 4.2.1 of Duan et al. (2023), we observed that $x_2 = x_1^2/x_0$ when $\beta_1 = 0$. If $\beta_1 > 0$, then by the P_*-diagram and Table 3, P_* does not lie in either $\mathcal{R}_{\text{R}_*}$ or $\mathcal{R}_{\text{C}_*}$. If P_* lies in $\mathcal{R}_{\text{G}_*}$ with $y_* > y_{01}$, then following the convention from Remark 1, we have A with $\sigma_A = [+ - + -]$, which contradicts that $\beta_1 > 0$. Therefore, $y_* < y_{01}$. Since $\beta_1 > 0$, whenever the trajectory $\varphi(t) = [x(t), y(t)]^\text{T}$ of (1) is above y_*, $\dot{x}$ is positive, and $\varphi(t)$ can thus be parametrized by x. Since P_2 lies in the rectangular region $[x_1, \infty) \times [y_1, \infty)$, the trajectory passes through P_1 transversely with x and y

both increasing. Therefore, if $y_* \le y_0$, then the trajectory is contained in the interior of the rectangle $\mathcal{R}^{(1)}_{\mathrm{NE}_2}$ when $t \in (0, 1)$ and in $(x_1, \infty) \times (y_1, \infty)$ when $t \in (1, 2)$. Thus, we have

$$\frac{\ln\left(\frac{x_1}{x_0}\right)}{\beta_1(y_1 - y_*)} < \int_{x_0}^{x_1} \frac{\mathrm{d}x}{\beta_1 x(y - y_*)} = 1 = \int_{x_1}^{x_2} \frac{\mathrm{d}x}{\beta_1 x(y - y_*)} < \frac{\ln\left(\frac{x_2}{x_1}\right)}{\beta_1(y_1 - y_*)}, \tag{30}$$

and hence $x_2 > x_1^2/x_0$. Alternatively, if $y_0 < y_* < y_{01}$, then within $t \in [0, 1]$, the trajectory progresses from P_0 in the direction of decreasing x and increasing y until $y(t) = y_*$; then continues in the direction of increasing x and y, reaching $x(t) = x_0$ again at some time $\tilde{t} \in (0, 1)$; and then continues in this direction until arriving at P_1 at time 1. Therefore, based on integration over the path traversed with $t \in (\tilde{t}, 1)$,

$$\frac{\ln\left(\frac{x_1}{x_0}\right)}{\beta_1(y_1 - y_*)} < \int_{x_0}^{x_1} \frac{\mathrm{d}x}{\beta_1 x(y - y_*)} = 1 - \tilde{t} < 1 = \int_{x_1}^{x_2} \frac{\mathrm{d}x}{\beta_1 x(y - y_*)} < \frac{\ln\left(\frac{x_2}{x_1}\right)}{\beta_1(y_1 - y_*)}, \tag{31}$$

and we see that $x_2 > x_1^2/x_0$ still holds.

Finally, suppose that $\beta_1 < 0$, such that by the P_*-diagram, Table 3, and Remark 1, $y_* > y_{01}$. The fact that P_2 lies above and to the right of P_1 implies that $\dot{x}|_{P_1} = \beta_1 x_1(y_1 - y_*)$ is positive, and hence $y_* > y_1$. Therefore in the x-direction, the trajectory increases when $t \in (0, 1)$ and continues doing so after $t = 1$ until $y(t) = y_*$. Regardless of the t value when $y(t) = y_*$, we always have

$$\frac{\ln\left(\frac{x_2}{x_1}\right)}{-\beta_1(y_* - y_1)} < \int_{x_1}^{x_2} \frac{\mathrm{d}x}{-\beta_1 x(y_* - y)} \le 1 = \int_{x_0}^{x_1} \frac{\mathrm{d}x}{-\beta_1 x(y_* - y)} < \frac{\ln\left(\frac{x_1}{x_0}\right)}{-\beta_1(y_* - y_1)},$$

so $x_2 < x_1^2/x_0$. □

Theorem 11 shows that the two curves $\mathcal{C}_{\beta_j=0}$, $j = 1, 2$ separate $[x_1, \infty) \times [y_1, \infty)$ into four quadrants. The signs of β_1, β_2 for solutions to the inverse problem differ across these quadrants, as in the P_2-diagram (Fig. 1) and corresponding Table 1.

Corollary 3 *(Uniqueness on $\mathcal{C}_{\beta_j=0}$) The inverse problem has a unique solution if either $x_2 = x_1^2/x_0$ and $y_2 \ge y_1$ both hold, or $x_2 \ge x_1$ and $y_2 = y_1^2/y_0$ both hold.*

Proof If $x_2 = x_1^2/x_0$ and $y_2 \ge y_1$, then $\beta_1 = 0$, which yields $x(t) = e^{\alpha_1 t} x_0$. Substitution of $x(2) = x_2 = x_1^2/x_0$ gives a unique formula for α_1. Moreover, in this case we can represent the solution curve as a graph over x of the function Duan et al. (2023)

$$y(x) = y_0 \exp\left(\frac{\alpha_2}{\alpha_1} \ln\left(\frac{x}{x_0}\right) + \frac{\beta_2}{\alpha_1}(x - x_0)\right).$$

Using this expression, it follows that the full parameter matrix A is given uniquely in terms of P_0, P_1 and y_2 as

$$A = \begin{bmatrix} \ln\left(\frac{x_1}{x_0}\right) & 0 & 0 \\ 0 & \frac{x_0}{(x_1-x_0)^2}\ln\left(\frac{x_1}{x_0}\right)\ln\left(\frac{y_0 y_2}{y_1^2}\right) & \frac{x_0}{x_0-x_1}\ln\left(\frac{y_2}{y_1}\right) - \frac{x_1}{x_0-x_1}\ln\left(\frac{y_1}{y_0}\right) \end{bmatrix}.$$

We can derive a similar result when $y_2 = y_1^2/y_0$ and $x_2 \geq x_1$. □

For the inverse problem for system (1), we have now proved the existence and uniqueness of solutions along some curves in the diagram and we have established σ_A for some regions. The remaining questions that we set out to answer were addressed numerically in earlier work (Duan et al. 2023), and their analytical treatment remains for future investigation.

6 Discussion

Overall, our analysis yields qualitative information about parameters and trajectories of the LV system (1) derived either from three data points on a single system trajectory, equidistant in time, or from two trajectory samples and the location of a positive equilibrium point. Our findings reveal that in the former scenario, nonuniqueness of compatible parameter sets can arise, related to folds in a manifold of inverse problem solutions, which could be an important property that generalizes to other nonlinear systems. In the latter, on the other hand, the mapping from the data to parameter values is one-to-one, although nonexistence of compatible parameter sets can still arise. Importantly, our analysis allows us to infer from the given data set whether the modeled species interact in a cooperative, competitive, or predator–prey type relationship and to characterize the sets of data positions that imply that the trajectories from which they were sampled engage in specific qualitative behaviors, such as periodic cycling.

Our approach does not rely on approximating the vector field explicitly or on the existence or properties of an attractor for the system under study, and we assume that the time step between data points is fixed, rather than being a factor that we can select to serve our aims. In our analysis of system (1), the quantity of data that we require is set by the number of parameters in the model, rather than by the attractor dimension; unlike the latter, the number of model parameters is known from the outset, which eliminates the need for additional experiments to estimate how much data will suffice. Although we assumed equal passage times between each pair of data points in our analysis, and the details of our findings depend on this assumption, our general approach does not require this equal spacing condition, and we expect that qualitative features of our results will persist for other measurement intervals.

A fundamental aspect of our inverse problem results is continuity: If we fix two of the data points, then there are regions in the (x, y) plane such that for all choices of the third data point within each region, the inverse problem solution is qualitatively the same; that is, existence and uniqueness properties persist throughout the region, as do the signs of the parameters that comprise such solutions. In a recent paper (Duan et al. 2023), we introduced a numerically generated illustration of our results in terms of these regions in data space, in what we call the P_2-diagram. Here, we establish a correspondence between these regions and the possible locations of the nontrivial equilibrium point of system (1), the knowledge of which, as an alternative to the third data point, also enables us to determine the properties of the inverse problem solution, as we display in what we call the P_*-diagram. Although rigorous results are derived here only for data satisfying condition (C), i.e., $x_0 < x_1$ and $y_0 < y_1$, P_2-diagrams corresponding to alternative choices of the relative positions of data points P_0 and P_1 can be found in Figure 10 of (Duan et al. 2023), and the methods presented here, including the reference to P_*-diagram can be easily extended to those cases.

Our results highlight that certain data points, with the specified timing, are incompatible with trajectories of system (1), and such nonexistence results can occur due to issues of timing or due to issues of trajectory curvature. In contrast to linear and affine systems (Stanhope et al. 2017; Duan et al. 2020), the region of nonexistence for the nonlinear system (1) is composed of several disconnected components. Our findings also show that some data points are compatible with distinct parameter sets giving rise to orbits that can be of the same type or of qualitatively different types, such as periodic versus unbounded orbits, with correspondingly similar or distinct biological interpretations of the associated parameter values, respectively. Although this situation occurred already in the case of linear and affine systems, here it is more remarkable as the present system has a first integral (a Hamiltonian). In these situations, additional data points or observations would be needed to indicate that the underlying biological system exhibits a specific type of inter-species interaction.

A natural question that can be asked about our qualitative findings is how robust they are to small changes in the locations of data points or to cases where we do not know that trajectories pass exactly through the given data but only that they pass within some neighborhoods of these points. The issue of robustness was addressed for linear and affine systems by exploration of the maximal permissible uncertainty of the data that would not change the implications for the qualitative behavior of solutions (Stanhope et al. 2017; Duan et al. 2020). Given the continuity of the P_2 diagram and its straightforward dependence on the location of the data points P_0, P_1, one can conjecture that the maximal permissible uncertainty for the LV system increases with the distance of the point P_2 from the boundary of the region in which it lies, but a more precise characterization will require further investigation.

Another possible research direction that we did not consider is to seek to identify what, if any, small changes to the dynamics of model (1) could result in a trajectory that passes through given data, when no such trajectory exists for (1) itself. This direction has been considered, for example, in past work on linear compartment models (Meshkat et al. 2015). Numerical results show that, as one would expect from the theory of structural stability and dependence of dynamical systems solutions on changes in parameter values (Perko 2013), variations of system (1) that can be represented in terms of parameter changes in a smoothly parameter-dependent vector field result in continuation of solution branches and continuous deformations of regions in the P_2-diagram (Duan et al. 2023); for example, such nice behavior occurs if we replace each xy interaction term with a parameter-dependent saturation of the form $xy/(\epsilon x + 1)$. Naturally, however, solution branches can fold, and bifurcations of regions in the P_2

diagram, such as the emergence of folds, can also occur; for the time being, we do not have a way to predict when these events will occur as a vector field parameter, such as ϵ in the above example, is varied. We also have not considered the case when measurements of only a proper subset of model variables are available, nor have we discussed the potentially interesting tradeoff between having less data about more variables versus more data about fewer variables.

Overall, our study stands as a unique and novel example of a thorough characterization of the set of inverse problem solutions for a specific canonical model in the study of population dynamics, which may prove helpful for researchers who use the LV model to study specific biological systems and can also serve as a starting point for further development of data-based analysis of dynamical systems. In such an approach, the dynamical behavior of the system and the continuation of a system trajectory are analyzed based on given data about the system variables at a small number of times, rather than being assessed based on specific parameter values for the system and the forward integration of the model with these values. Within the space of data, one identifies regions that correspond to various types of model behavior, with borders between those regions serving the same purpose as bifurcation curves would in traditional analysis from a parameter space perspective. In future explorations of this subject, we expect that a more comprehensive theory of data-based model analysis can be developed, with methods and techniques that will be applicable to additional classes of nonlinear dynamical systems.

References

Aster RC, Borchers B, Thurber CH (2018) Parameter estimation and inverse problems. Elsevier, Amsterdam

Broomhead DS, King GP (1986) Extracting qualitative dynamics from experimental data. Physica D 20(2–3):217–236

Calvetti D, and Somersalo E (2007) An introduction to bayesian scientific computing: ten lectures on subjective computing (Vol. 2). Springer Science & Business Media

Calvetti D, Somersalo E (2018) Inverse problems: from regularization to Bayesian inference. Wiley Interdiscip Rev Comput Stat 10(3):e1427

Cao J, Wang L, Xu J (2011) Robust estimation for ordinary differential equation models. Biometrics 67(4):1305–1313

Dalgaard P, and Larsen M (1990) Fitting numerical solutions of differential equations to experimental data: a case study and some general remarks. Biometrics, 1097–1109

Duan X, Rubin J, Swigon D (2020) Identification of affine dynamical systems from a single trajectory. Inverse Prob 36(8):085004

Duan X, Rubin JE, Swigon D (2023) Qualitative inverse problems: mapping data to the features of trajectories and parameter values of an ODE model. Inverse Prob, 39:075002

Evensen G (2009) Data assimilation: the ensemble kalman filter. Springer Science & Business Media

Fort H (2018) On predicting species yields in multispecies communities: quantifying the accuracy of the linear Lotka-Volterra generalized model. Ecol Modell 387:154–162

Khan T, Chaudhary H (2020) Estimation and identifiability of parameters for generalized Lotka-Volterra biological systems using adaptive controlled combination difference anti-synchronization. Differ Eq Dyn Syst 28(3):515–526

Kloppers P, Greeff J (2013) Lotka-Volterra model parameter estimation using experiential data. App Math Comput 224:817–825

Kunze H, Hicken J, Vrscay E (2004) Inverse problems for odes using contraction maps and suboptimality of the? Collage method? Inverse Probl 20(3):977

Lazzus JA, Vega-Jorquera P, Lopez-Caraballo CH, Palma-Chilla L, Salfate I (2020) Parameter estimation of a generalized Lotka-Volterra system using a modified PSO algorithm. Appl Soft Comput 96:106606
MacKay RS, Meiss JD (2020) Hamiltonian dynamical systems: a reprint selection. CRC Press, Boca Raton, FL
May RM (ed) (1976) Theoretical ecology: principles and applications. Elsevier - Health Sciences Division, Amsterdam
Meshkat N, Sullivant S, Eisenberg M (2015) Identifiability results for several classes of linear compartment models. Bull Math Biol 77(8):1620–1651
Packard NH, Crutchfield JP, Farmer JD, Shaw RS (1980) Geometry from a time series Geometry from a time series. Phys Rev Lett 45(9):712
Perko L (2013) Differential equations and dynamical systems, vol 7. Springer Science & Business Media, New York, NY
Ramsay JO, Hooker G, Campbell D, Cao J (2007) Parameter estimation for differential equations: a generalized smoothing approach. J Royal Stat Soci Series B (Stat Methodol) 69(5):741–796
Smith RC (2013) Uncertainty quantification: theory, implementation, and applications, vol 12. SIAM, Philadelphia, PA
Stanhope S, Rubin J, Swigon D (2014) Identifiability of linear and linear-in-parameters dynamical systems from a single trajectory. SIAM J Appl Dyn Syst 13(4):1792–1815
Stanhope S, Rubin J, Swigon D (2017) Robustness of solutions of the inverse problem for linear dynamical systems with uncertain data. SIAM/ASA J Uncertain Quantif 5(1):572–597
Stuart AM (2010) Inverse problems: a Bayesian perspective. Acta Numer 19:451–559
Swigon D, Stanhope SR, Zenker S, Rubin JE (2019) On the importance of the Jacobian determinant in parameter inference for random parameter and random measurement error models. SIAM/ASA J Uncertain Quantif 7(3):975–1006
Takens F (1981) Dynamical systems and turbulence, Warwick 1980. Heidelberg, Springer, Berlin, pp 366–381
Tarantola A (2005) Inverse problem theory and methods for model parameter estimation. SIAM
Wangersky PJ (1978) Lotka-Volterra population models. Annu Rev Ecol Syst 9:189–218
Wu L, Wang Y (2011) Estimation the parameters of Lotka-Volterra model based on grey direct modelling method and its application. Expert Syst Appl 38(6):6412–6416